JOURNAL OF COMPUTATIONAL PHYSICS **124,** 192–216 (1996)
ARTICLE NO. 0053

Computational Methods for Propagating Phase Boundaries

XIAOGUANG ZHONG,*,[1] THOMAS Y. HOU,†,[2] AND PHILIPPE G. LEFLOCH‡,[3]

*Department of Applied Mechanics, 104-44 and †Department of Applied Mathematics, 217-50, Division of Engineering and Applied Science, California Institute of Technology, Pasadena, California 91125; ‡Department of Mathematics, Center for Applied Mathematical Sciences, University of Southern California, Los Angeles, California

Received March 13, 1995; revised July 19, 1995

This paper considers numerical methods for computing propagating phase boundaries in solids described by the physical model introduced by Abeyaratne and Knowles. The model under consideration consists of a set of conservation laws supplemented with a kinetic relation and a nucleation criterion. Discontinuities between two different phases are undercompressive crossing waves in the general terminology of nonstrictly hyperbolic systems of conservation laws. This paper studies numerical methods designed for the computation of such crossing waves. We propose a Godunov-type method combining front tracking with a capturing method; we also consider Glimm's random choice scheme. Both methods share the property that the phase boundaries are sharply computed in the sense that there are no numerical interior points for the description of a phase boundary. This property is well known for the Glimm's scheme; on the other hand, our front tracking algorithm is designed so that it tracks phase boundaries but captures shock waves. Phase boundaries are sensitive to numerical dissipation effects, so the above property is essential to ensure convergence toward the correct entropy weak solution. Convergence of the Godnuov-type method is demonstrated numerically. Extensive numerical experiments show the practical interest of both approaches for computations of undercompressive crossing waves.

CONTENTS

1. INTRODUCTION

After Ericksen's seminal paper [19], continuum modeling of solid–solid phase transformations by finite elasticity theory has been a very active research area in the community of continuum mechanics. Now it is known that a nonlinear elastic material capable of phase transformation can be modeled by a nonconvex free energy function (cf., for a background on the subject, Abeyaratne [1] and Rosakis [54]). The loss of convexity, or more generally of rank-one convexity of a free energy function (which would imply nonstrong ellipticity for the set of P.D.E's) leads to nonuniqueness of solutions to the corresponding boundary value problem or initial-boundary value problem, even if entropy admissibility conditions are imposed; cf. James [34]. In the setting of continuum mechanics, the nonuniqueness of solutions can be viewed as a lack of constitutive information about the phase transformation process. In order to recover a unique solution to a boundary value problem or initial-boundary value problem, various constitutive postulates have been proposed; typically one requires that the solution minimize the total energy in a suitable sense (Dafermos [18], Ericksen [19], Ball and James [7]), or be obtained as the limit of a viscosity regularization of the set of P.D.E.'s (Slemrod [61], Fan-Slemrod [20], Rybka [55], Swart and Holmes [62]).

Another approach was recently proposed by Abeyaratne and Knowles [2–5], who introduced postulates of constitutive nature at phase boundaries. The Abeyaratne–Knowles approach deals primarily with the quasi-statics and dynamics of phase transformation. Moreover, this model is able to describe the solutions obtained by the viscosity regularization theory in certain sense (Abeyaratne and Knowles [5] and, for a mathematical setting, LeFloch [41]). The objective of this paper is to present two numerical methods suitable to compute the solutions to initial-boundary-value problems associated with the Abeyaratne–Knowles model.

[1] E-mail: zhong@cco.caltech.edu; address after August 15, 1995: Department of Engineering Science and Mechanics, Virginia Polytechnic Institute and State University, Blacksburg, VA 24061.
[2] E-mail: hou@ama.caltech.edu.
[3] E-mail: lefloch@cams.usc.edu.

0021-9991/96 $18.00

The materials we deal with are characterized by nonconvex strain energy functions. These materials describe both stable deformations and metastable deformations. Phases are associated with disjoint deformation domains of a single strain energy function. In each disjoint deformation domains, a deformation is either stable, metastable, or unstable. Based on the fact that an unstable deformation is not observable in solid–solid phase transformations, it is assumed that a deformation will jump from one stable or metastable phase to another when a certain critical value is reached. Such an occurrence leads to the formation of a phase boundary, or nucleation. The emergence of a new phase boundary is a consequence of the local instability of a deformation. The basic assumptions in the Abeyaratne–Knowles model are as follows:

(i) The deformation is smooth enough, say of class C^2, away from shock fronts or phase boundaries. Deformation gradients are discontinuous across shock fronts or phase boundaries, but the deformation itself should be continuous.

(ii) Two supplementary constitutive relations are postulated: a *kinetic relation* valid at any subsonic phase boundaries and a *nucleation criterion.*

Thus phase boundaries are not free boundaries, but rather are driven by the kinetics. Unlike classical shock waves, phase boundaries should not be viewed as a consequence of overlapping characteristics. In other words phase boundaries do not arise dynamically, but instead are created spontaneously when certain conditions are fulfilled.

Since the P.D.E.'s describing the dynamics of phase transformations are nonlinear, the initial-boundary value problems cannot be solved analytically in general, and developing computational methods is therefore an important task.

Numerical methods developed in the last 10 years for classical shock waves in CFD cannot be applied directly to phase boundary propagation problems. A phase boundary indeed has distinct properties as we will explain it below. However, we are able to build upon numerical techniques developed in CFD and develop an efficient and robust numerical method capable of computing dynamical phase transition problems.

There are two types of classical methods for shock wave computations. They can be classified as shock tracking and shock capturing schemes.

(i) *The front tracking schemes*. For the recent activity on the subject, we can refer to Glimm *et al.* [24, 25], Hyman [32], Moretti [49], and Oran and Boris [51]. See also the works by Chern and Colella [12] and LeVeque and Shyue [42]. A main advantage of the front tracking methods lies in the fact that the shock front is sharply computed basically without any numerical dissipation. However, the implementation of such a method is more difficult if complex flow features such as shock wave interactions must be taken into account.

(ii) *The shock capturing schemes,* which represent a more standard methodology. In particular the first-order accurate Godunov method [26] and its higher order extensions have received a lot of attention in recent years. This research culminated with works by van Leer [40] (MUSCL scheme), Colella and Woodward [16] (PPM scheme), Harten, Osher *et al.* [28, 30, 52] (ENO schemes), and others. The implementation of shock capturing methods is generally straightforward. Shock fronts are not sharply computed, but they usually spread out over a few mesh cells only; this is satisfactory for most applications. Several methods that further sharpen numerical shock fronts have been developed; see Harten and Hyman [27] for a self-adjusting grid method and Harten [29] for the technique of subcell resolution applied to ENO schemes. To combine the advantages of tracking and capturing methods, it may be advantageous to hybridize the two techniques: tracking strong shock waves but capturing those with weak strength [11, 12, 58].

Various numerical methods have been applied to computing the dynamics of solid–solid phase transformations. Kloucek and Luskin [37] and Swart and Holmes [62] used finite difference or finite element methods, combined with various type of either physically motivated or artificial viscosity regularizations. The phase boundary in this approach is spread over a narrow region. Slemrod [61] performed numerical experiments with the Lax–Friedrichs scheme. Various finite difference techniques have been considered by Affouf and Caflisch [6], Cockburn and Gau [14], and Jin [35]. Silling used a dynamical relaxation technique to model quasi-static phase transformation processes and the dynamic growth of martensitic plates [59, 60]. We also refer to the works by Collins and Luskin [17] and Nicolaides and Walkington [50].

The present paper deals with the model recently introduced by Abeyaratne and Knowles. The system of P.D.E.'s in the model takes the form of a hyperbolic-elliptic system of 2×2 conservation laws in the one-dimensional setting. The class of materials considered here admits a nonmonotone stress–strain relation; this leads to an elliptic region separating two hyperbolic regions. Based on the physical origin of the system, it is natural to restrict attention to the hyperbolic regions. Abeyaratne and Knowles [5] have shown that the Riemann problem for this system is well posed, provided the initial data take values in the hyperbolic regions only, and the conservation laws are supplemented with an entropy inequality, a *kinetic relation*, and an *initiation criterion.*

For material on nonstrictly hyperbolic equations, we refer to the paper by Isaacson, Marchesin, and Plohr [33]

and the references therein. The phase boundaries are interpreted as *undercompressive crossing waves*; an analysis of the characteristics associated with the system shows that such waves are not uniquely determined by their initial data even if the Lax entropy inequality (or Clausius–Duhem principle) is imposed. Cf. Dafermos [18] for a review on the entropy criterion. Stability of undercompressive waves is an active area of research; cf. Liu and Zumbrum [44]. Cf. also Shearer [56], Keyfitz [36], and Truskinovsky [63] for additional materials on the system.

Two main questions we have to address for designing a scheme adapted to propagating phase boundaries are the following ones:

(i) How to incorporate in the scheme the kinetic relation which drives the motion of a phase boundary?

(ii) How to avoid the unstable deformation domain of the strain energy function?

To overcome these difficulties, we propose a front tracking/capturing method. In this method, conventional shock waves will be captured, but phase boundaries will be tracked by solving locally the Riemann solution which includes the effect of the kinetic relation and the nucleation criterion. By tracking the phase boundaries explicitly, we avoid computing cell averages over quantities in different phases. As a consequence, cell average values falling in an unstable phase are excluded. This is very important for the stability of our numerical method.

In this paper, we first focus on a special elastic material capable of phase transition, the so-called trilinear material. The Riemann solution for this trilinear material can be obtained analytically, and the properties of the solutions are relatively well understood. We also extend our numerical method to include more general two-phase elastic materials. For general two-phase elastic materials, the Riemann problem in general cannot be solved analytically. An approximate Riemann solver must be constructed. Standard method, such as Roe's approximate Riemann solver cannot be used directly here, due to the nonconvexity of the strain energy function. Here we propose a possible extension of Roe's solver to the phase transformation problem. This approximate Riemann solver shares many properties of Roe's solver for conventional conservation laws. Preliminary numerical experiments seem to give favorable results.

Another method which is capable of computing propagation of phase boundaries is the random-choice scheme introduced by Glimm in [22]. The convergence of this method for phase/capturing method and the Glimm scheme share the property that the phase boundaries are sharply computed in the sense that there are no numerical interior points for describing a phase boundary. This property is essential to ensure the convengence to the correct entropy weak solution. To demonstrate the relevance of both methods considered in the present paper, we apply them to various practical situations: notably, the propagation of a phase boundary in a Riemann problem and the propagation of a phase boundary in a finite domain (which is an initial-boundary value problem). We also compute the nucleation of a new phase and the collision of two phase boundaries. The numerical results are in excellent agreement with the analytical solutions when available.

By developing a Godunov-type front tracking/capturing method, we make it possible to solve arbitrary initial-boundary value problems; in particular, our method can be used to compare the predictions of the model to experimental observations in complex physical situations. On the other hand, the numerical method can also be applied to check the physical model itself, e.g., to decide whether time-dependent solutions approach stationary solutions in the long run. Furthermore, the techniques and ideas in this paper could be applied to other systems admitting undercompressive crossing waves. It should be noted that Mamiya and Simo [45] recently developed a finite element method for the Abeyaratne–Knowles model. But they only considered the quasi-static case (i.e., inertial term neglected) for a special kinetic relation.

The outline of this paper is as follows. In Section 2, we introduce the model proposed by Abeyaratne and Knowles, and we list some solutions to the Riemann problems. Section 3 presents our front tracking/capturing method that accommodates the kinetic relation and the nucleation criterion. Section 4 discusses Glimm's scheme. In Section 5, we extend our front tracking/capturing method to include more general two-phase elastic materials by proposing an approximate Riemann solver. Section 6 presents several numerical experiments. We make several remarks about this work in conclusion.

2. MODELING OF PROPAGATING PHASE BOUNDARIES

2.1. The Abeyaratne–Knowles Model

Consider a one-dimensional bar with uniform cross section A and uniform mass density ρ that occupies the interval $[0, L]$ in an unstressed reference configuration. In a longitudinal motion of the bar, the particle at x is carried to the point $x + u(x, t)$ at time t, where the displacement u is assumed to be Lipschitz continuous and have piecewise first and second derivatives on $[0, L]$ for each $t > 0$. We denote by

$$\gamma = u_x, \quad v = u_t, \tag{2.1}$$

the strain and particle velocity, respectively. It is assumed that $\gamma(x, t) > -1$ so that the mapping $x \to x + u(x, t)$ is invertible at each time t. The following stress–strain function is a given constitutive relation depending on the material under consideration:

$$\sigma = \sigma(\gamma). \tag{2.2}$$

Neglecting body forces for simplicity, the equations of motion and the compatibility read as follows:

$$\sigma'(\gamma)\gamma_x - \rho v_t = 0, \tag{2.3}$$

$$v_x - \gamma_t = 0. \tag{2.4}$$

Equations (2.3)–(2.4) take the form of 2×2 system of conservation laws:

$$U_t + f(U)_x = 0, \quad U = \begin{pmatrix} v \\ \gamma \end{pmatrix}, \quad f(U) = \begin{pmatrix} -\sigma(\gamma)/\rho \\ -v \end{pmatrix}. \tag{2.5}$$

We shall be concerned with traveling discontinuities for system (2.5). If there is a strain discontinuity at $x = s(t)$, the following jump conditions must hold:

$$\dot{s}(\gamma_+ - \gamma_-) = -(v_+ - v_-), \tag{2.6}$$

$$\sigma(\gamma_+) - \sigma(\gamma_-) = -\rho\dot{s}(v_+ - v_-), \tag{2.7}$$

where the index $\pm$ denotes limiting values in front of and behind the discontinuity, respectively. Let

$$W(\gamma) = \int_0^\gamma \sigma(\gamma')\, d\gamma' \tag{2.8}$$

be the strain energy per unit volume. For definiteness, let us consider the restriction of the motion to the time interval $[t_1, t_2]$ and the piece of the bar that occupies the interval $[x_1, x_2]$ in the reference configuration. Suppose that γ and v are smooth functions for $x \in [x_1, x_2]$ and $t \in [t_1, t_2]$ everywhere except along a curve of discontinuity $x = s(t)$.

Let $E(t)$ be the total mechanical energy at time t for the piece of the bar under consideration:

$$E(t) = \int_{x_1}^{x_2} [W(\gamma(x,t) + \tfrac{1}{2}\rho v^2(x,t)]A\, dx. \tag{2.9}$$

A direct calculation based on Eqs. (2.5) establishes the following work-energy identity:

$$\sigma(x_2)v(x_2,t)A - \sigma(x_1)v(x_1t)A - \dot{E}(t) = f(t)\dot{s}(t)A, \tag{2.10}$$

where the *driving traction* $f(t)$ is defined by

$$f(t) = \hat{f}(\gamma_-, \gamma_+) = \int_{\gamma_-}^{\gamma_+} \sigma(\gamma)\, d\gamma - \tfrac{1}{2}[\sigma(\gamma_+) + \sigma(\gamma_-)](\gamma_+ - \gamma_-). \tag{2.11}$$

The admissibility entropy condition satisfied by any propagating wave, and especially the phase boundary, is

$$f(t)\dot{s}(t) \geq 0. \tag{2.12}$$

Under isothermal conditions, the admissibility condition is a consequence of the second law of thermodynamics. For reference, see, for example, [38].

A Material Capable of Phase Transition. The Jacobian matrix of system (2.5) has the form

$$\nabla f(U) = \begin{pmatrix} 0 & -\dfrac{\sigma'(\gamma)}{\rho} \\ -1 & 0 \end{pmatrix}$$

and therefore admits two (real or complex eigenvalues: $\pm(\sigma'(\gamma)/\rho)^{1/2}$. In this paper, the stress-strain function is assumed to have the following properties:

$$\sigma(\gamma) \text{ is monotone increasing for } \gamma \in (-1, \gamma_m) \cup (\gamma_M, \infty), \tag{2.13}$$

$$\sigma(\gamma) \text{ is monotone decreasing for } \gamma \in (\gamma_m, \gamma_M), \tag{2.14}$$

where γ_M and γ_m are fixed constants satisfying $-1 < \gamma_m < \gamma_M$. It follows that system (2.5) admits two real eigenvalues $\pm(\sigma'(\gamma)/\rho)^{1/2}$ if either $\gamma \in (-\infty, \gamma_m) \equiv H_1$ or $\gamma \in (\gamma_M, +\infty) \equiv H_3$. In the range of values (γ_m, γ_M), the eigenvalues are not real, and the system (2.5) is elliptic. The latter region corresponds to unstable deformation and is excluded. In the whole of this paper, only values of γ in $H_1 \cup H_3$ will be dealt with.

The simplest materials capable of phase transformations are the so-called *trilinear materials.* This choice has been proposed in [5] in order to carry out analytical calculations. We focus primarily on the trilinear materials in this paper. The trilinear stress-strain relation is

$$\sigma(\gamma) = \begin{cases} \mu\gamma, & -1 < \gamma < \gamma_m, \\ \dfrac{\sigma_m - \sigma_M}{\gamma_m - \gamma_M}(\gamma - \gamma_M) + \sigma_M, & \gamma_m < \gamma < \gamma_M, \\ \mu(\gamma - \gamma_T), & \gamma_M < \gamma, \end{cases} \tag{2.15}$$

where $\sigma_m = \mu\gamma_m$, $\sigma_M = \mu(\gamma_M - \gamma_T)$. We call $-1 < \gamma < \gamma_m$ phase 1, $\gamma_m < \gamma < \gamma_M$ phase 2, and the rest phase 3. Phase 1 and 3 are metastable phases; phase 2 is an unstable phase. Typically phase 1 identifies itself with the phase of austenite, and phase 3 with the phase of martensite. Waves in each phase propagate with speed $c = (\mu/\rho)^{1/2}$. The driving traction on a 3–1 phase boundary is derived from (2.11):

$$f(\gamma_-, \gamma_+) = \frac{\mu\gamma_T}{2}(\gamma_+ + \gamma_- - \gamma_M - \gamma_m). \qquad (2.16)$$

One can check that the system (2.5) has self-similar solutions which are not uniquely determined by the jump conditions, the entropy admissibility condition (2.12), and the initial condition. In fact subsonic phase boundaries are undercompressive crossing shocks in the general terminology of systems of conservation laws. For such waves, it is expected that the classical admissibility conditions are not enough to determine the solutions. Supplementary conditions derived from the physics are necessary.

Two Supplementary Constitutive Relations. Besides the equations of motion, stress–strain relation, jump conditions, and admissibility condition, we must specify two supplementary constitutive relations in order to uniquely determine a solution of the system. The two supplementary constitutive relations are the kinetic relation and the nucleation criterion. The kinetic relation relates the phase boundary propagation speed $\dot{s}$ to the driving traction $f(t)$ acting on the phase boundary. The nucleation criterion determines when a new phase will nucleate from the parent phase. These two relations are material-dependent. In the present paper, we shall use the following kinetic relation and nucleation criterion:

1. Kinetic relation:

$$f = \phi_{pq}(\dot{s}) \qquad (2.17)$$

for a phase boundary propagating from phase p to phase q, where $\phi_{pq}(\dot{s})$ is a monotonically increasing function that may be discontinuous at $\dot{s} = 0$ and satisfies $\phi_{pq}(\dot{s})\dot{s} \geq 0$.

2. Nucleation criterion. Generally speaking the nucleation criterion should be expressed in terms of the driving traction. However, for trilinear materials the nucleation criterion can be formulated in terms of strain which is more convenient to use, say

$$\gamma \geq \gamma_{\text{cr}} \qquad (2.18)$$

for phase 1 to phase 3 transformation and

$$\gamma \leq \gamma^*_{\text{cr}} \qquad (2.19)$$

for phase 3 to phase 1 transformation, where γ^*_{cr} and γ_{cr} are given constants, called critical transformation strains.

Observe that only the entropy condition (2.12) imposes some restriction on the kinetic response function $\phi_{pq}(\dot{s})$. These kinetic response functions may be supplied by appropriate constitutive modeling; an example is provided by the thermal activation theory [64]. The special choice of the function $\phi_{pq}(\dot{s}) = 0$ would be obtained from a model with dissipation-free phase boundaries. One could also postulate that $\phi_{pq}(\dot{s}) = \omega\dot{s}$, where ω is a sufficiently small positive constant. This postulated kinetic response function can be viewed as a linearization of the kinetic response function derived by thermal activation theory.

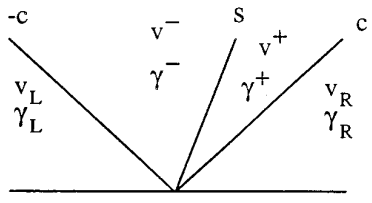

FIG. 1. Form of solution to Riemann problem with 1–3 initial data.

The form of nucleation criterion is motivated, in part, by models used to describe nucleation in materials science; see, e.g., Christian [13], Fine [21]. Roughly speaking, when a new phase is to be nucleated from its parent phase, the transformed material of the parent phase has to overcome certain "energy barrier." The "energy barrier" can be overcome when the local driving force is large enough.

2.2. Riemann and Goursat–Riemann Problems

This section provides us with some explicit solutions to the Abeyaratne–Knowles model that will be useful to test the numerical methods presented in this paper. For additional details, we refer to Abeyaratne and Knowles [4] and Zhong [65]. We refer to LeFloch [41] for the continuous dependence of the solutions.

Consider the initial data:

$$v(x,0), \gamma(x,0) = \begin{cases} v_L, \gamma_L, & -\infty < x < 0, \\ v_R, \gamma_R, & 0 < x < \infty, \end{cases} \qquad (2.20)$$

for our set of Eqs. (2.5)–(2.7), supplemented with the trilinear material in Section 2.1.

The solutions to the Riemann problem are listed for two cases of interest.

Case I. A 1–3 initial data; i.e., γ_L is in phase 1 and γ_R is in phase 3. The Riemann solution then contains a single phase boundary; cf. Fig. 1. The solution has the form

$$v(x,t), \gamma(x,t) = \begin{cases} v_L, \gamma_L, & -\infty < x < -ct, \\ v_-, \gamma_-, & -ct < x < \dot{s}t, \\ v_+, \gamma_+, & \dot{s} < x < ct, \\ v_R, \gamma_R, & ct < x < \infty, \end{cases} \qquad (2.21)$$

here the intermediate states are given by

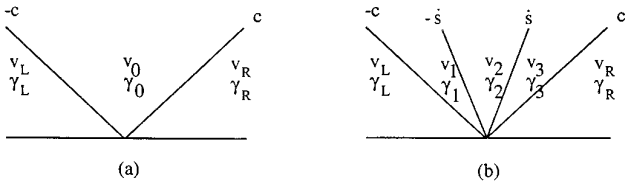

FIG. 2. Form of solutions to Riemann problem with 1–1 initial data: (a) no new phase boundaries; (b) two phase boundaries.

$$\gamma_- = h - \frac{c\gamma_T}{2(c+\dot{s})},$$
$$v_- = v_L + c(\gamma_- - \gamma_L),$$
$$\gamma_+ = h + \frac{c\gamma_T}{2(c-\dot{s})},$$
$$v_+ = v_R - c(\gamma_+ - \gamma_R),$$
$$h = \frac{1}{2c}(v_R - v_L + c(\gamma_R + \gamma_L)).$$

Here $\dot{s}$ is determined by the kinetic relation at the phase boundary, $f = \phi_{13}(\dot{s})$, i.e.,

$$\frac{\mu\gamma_T}{2}(\gamma_m + \gamma_M - \gamma_- - \gamma_+) = \phi_{13}(\dot{s}). \tag{2.22}$$

Case II. A 1–1 initial data; i.e., γ_L and γ_R are in phase 1. We distinguish here two cases. If $(1/2c)(v_R - v_L + c(\gamma_R + \gamma_L)) \le \gamma_{\mathrm{cr}}$, then the solution is

$$v(x,t), \gamma(x,t) = \begin{cases} v_L, \gamma_L, & -\infty < x < -ct, \\ v_0, \gamma_0, & -ct < x < ct, \\ v_R, \gamma_R, & ct < x < \infty, \end{cases} \tag{2.23}$$

where

$$\gamma_0 = \frac{1}{2c}(v_R - v_L + c(\gamma_R + \gamma_L)),$$
$$v_0 = v_L + c(\gamma_0 - \gamma_L)$$

(see Fig. 2a).

If $(1/2c)(v_R - v_L + c(\gamma_R + \gamma_L)) > \gamma_{\mathrm{cr}}$, then there is a new phase initiated at the origin; see Fig. 1b. The solution is

$$v(x,t), \gamma(x,t) = \begin{cases} v_L, \gamma_L, & -\infty < x < -ct, \\ v_1, \gamma_2, & -ct < x < \dot{s}t, \\ v_2, \gamma_2, & -\dot{s}t < x < \dot{s}t, \\ v_3, \gamma_3, & \dot{s}t < x < ct, \\ v_R, \gamma_R, & ct < x < \infty, \end{cases} \tag{2.24}$$

where

$$\gamma_1 = h - \frac{c\dot{s}\gamma_T}{c^2 - \dot{s}^2},$$
$$\gamma_2 = h + \frac{c\gamma_T}{c+\dot{s}},$$
$$\gamma_3 = h - \frac{c\dot{s}\gamma_T}{c^2 - \dot{s}^2},$$
$$v_1 = v_L - c\gamma_L + ch - \frac{c^2\dot{s}\gamma_T}{c^2 - \dot{s}^2},$$
$$v_2 = v_L - c\gamma_L + ch,$$
$$v_3 = v_R + c\gamma_R - ch + \frac{c^2\dot{s}\gamma_T}{c^2 - \dot{s}^2},$$
$$h = \frac{1}{2c}(v_R - v_L + c(\gamma_R + \gamma_L)).$$

Here $\dot{s}$ is determined by the kinetic relation at a phase boundary, $f = \phi_{13}(\dot{s})$.

We now turn to the Goursat–Riemann problem characterized with the initial conditions

$$v(x,0) = v_0, \quad 0 < x < \infty,$$
$$\gamma(x,0) = \gamma_0, \quad 0 < x < \infty,$$

and a boundary condition for the velocity,

$$v(0,t) = v_b, \quad 0 < t < \infty,$$

where γ_0, v_0, v_b are given constants; see Fig. 3.

Observe that it would be equivalent to impose a boundary condition on the displacement. We can also impose the traction: $\sigma(0,t) = \sigma_0$, which is equivalent to imposing the strain.

Case I. The material is initially in phase 1, i.e., $\gamma_0 < \gamma_{\mathrm{cr}}$. If $v_b > v_0 + c(\gamma_0 - \gamma_{\mathrm{cr}})$, then the solutions are (Fig. 3a):

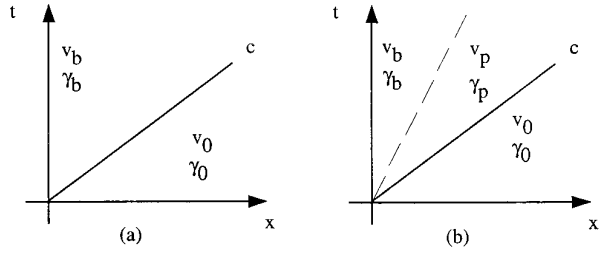

FIG. 3. Form of solutions to a Goursat–Riemann problem: (a) nonnew phase boundary; (b) one phase boundary.

$$v(x,t), \gamma(x,t) = \begin{cases} v_b, \dfrac{v_0 - v_b}{c} + \gamma_0, & 0 < x < ct, \\ v_0, \gamma_0, & ct < x < \infty. \end{cases} \tag{2.25}$$

If $v_b < v_0 + c(\gamma_0 - \gamma_{\mathrm{cr}})$, then the solution is (Fig. 3b)

$$v(x,t), \gamma(x,t) = \begin{cases} v_b, \gamma_b, & 0 < x < \dot{s}t, \\ v_p, \gamma_p, & \dot{s}t < x < ct, \\ v_0, \gamma_0, & ct < x < \infty. \end{cases} \tag{2.26}$$

where

$$\gamma_b = \frac{v_0 + c\gamma_0}{c} - \frac{v_b}{c} + \frac{c\gamma_T}{c + \dot{s}},$$

$$v_p = v_b + \frac{c^2 \dot{s} \gamma_T}{c^2 - \dot{s}^2},$$

$$\gamma_p = \frac{v_0 + c\gamma_0}{c} - \frac{v_b}{c} - \frac{c\dot{s}\gamma_T}{c^2 - \dot{s}^2}.$$

Again $\dot{s}$ is determined by the kinetic relation.

Case II. The material is initially in phase 3, i.e., $\gamma_0 > \gamma_{\mathrm{cr}}^*$. The formula for the solution for this case is very similar to the one of Case I, so we omit it.

3. A FRONT TRACKING/CAPTURING METHOD

3.1. The General Approach

Our objective is to present a numerical method for the computation of dynamical phase transition problems. As the solutions of the Riemann problem are known explicitly, it is natural to develop a Godunov-type method. The standard Godunov method in principle could be applied; however, it does not produce the correct solution. We observe that a phase boundary is rather different from a conventional shock wave and numerical methods for shock waves cannot be applied directly. Our objective is to design a method that does not introduce numerical values in the unstable region of system (2.5), that is, in the interval (γ_m, γ_M). This will be achieved by using a Lagrangian algorithm in which the interface is tracked. Below we briefly review Godunov's method and explain how it has to be modified to meet present needs. We use the following notation. As variable meshes will be used, we denote by $x_{j+1/2}^n$ the spatial grid points at time t_n. Subsequently $[x_{j-1/2}^n, x_{j+1/2}^n]$ represents a computational cell, x_j^n is the center of the cell, and $h_j^n = x_{j-1/2}^n - x_{j+1/2}^n$ is the cell width at time t_n. We denote by k_n the nth time step, and we set: $t_n = \sum_{m=1}^{n-1} k_m$, $t_0 = 0$. If $U(t, x)$ is given, the cell average of U in the cell j and at time t_n is defined as

$$U_j^n = \frac{1}{h_j^n} \int_{x_{j-1/2}^n}^{x_{j+1/2}^n} U(t_n, x)\, dx. \tag{3.1}$$

Given the approximate solution $\{U_j^n\}$ at time t_n, the Godunov scheme consists of two main steps:

(i) Solve a Riemann problem at each cell interface $x_{j-1/2}^n$ with the initial data (U_{j-1}^n, U_j^n) $(j = ..., -1, 0, 1, ...)$. The solution at the time $t = t_{n+1}$ is known on the whole space interval and locally in time, that is, at least in the interval $[t_n, t_{n+1}]$.

(ii) Compute the cell averages at time t_{n+1} in each computational cell and obtain $\{U_j^{n+1}\}$.

Step (i) can be performed for a phase boundary problem in the same way that it is done for a problem admitting conventional shock waves only. The Riemann solution, including the effect of the kinetic relation and the nucleation criterion, is known explicitly. Step (ii), however, should not be carried out when a cell contains the two possible phases.

In designing our Godunov scheme for propagating phase boundaries, it is important to avoid computing an average over quantities in different phases. As a matter of fact, if we do compute averages over quantities in different phases, we may get a value for the strain falling in an unstable phase—unstable phases do not arise in the physical model if initial data are metastable. Such values may lead to instability in the computation. To avoid computing the average over a phase mixture, we must know the position of a phase boundary exactly so that we can somehow compute the average entirely in one phase. When we are away from the phase boundaries, we want to take the advantage of shock capturing schemes. So our strategy is to develop a front tracking/capturing method that tracks phase boundaries and captures conventional shock waves.

The method reads as follows: the space is discretized in such a way that a phase boundary is at a grid point (a cell interface). If at some time t_n a phase boundary is located at one grid point, the computation will proceed as follows:

(i) Compute all quantities at the time t_{n+1} from the approximation at the time t_n, including the phase boundary propagation speed determined by the kinetic relation and the location of the phase boundary at t_{n+1}.

(ii) Shift the grid mesh according to the movement of the phase boundary so that the phase boundary is still a grid point.

This approach is typical of the so-called Lagrangian algorithms. To implement the idea, a moving mesh has to be used. The method will be presented in three steps: first an algorithm for an initial value problem with a single phase boundary will be described. In a second stage it will be extended to the initial-boundary value problem. Then the

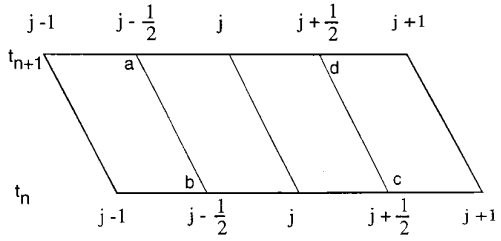

FIG. 4. A mesh in (x, t) plane.

algorithm will be further modified to include the nucleation of new phase boundaries at the boundary of, or inside, the computational domain and the possible collision of two phase boundaries. For definiteness, we shall restrict the presentation of the method to the case that Riemann solutions only involve 1–3 initial data. Assume that at the time t_n an approximation of the solution is known and the phase boundary occupies a grid point. The speed of the phase boundary at the time t_n will be denoted by V^n. As seen in Section 2.2, it is determined from the kinetic relation by solving a Riemann problem. As a consequence, the location of the phase boundary is known. At the time t_{n+1}, the mesh is shifted uniformly according to: $x_{j+1/2}^{n+1} = x_{j+1/2}^n + V^n k_n$. An explicit formula for the scheme can be derived in the following way.

Consider an element T (abcd) about the cell j in (x, t) plane (Fig. 4). Integrate the conservation laws (2.5) over the element T:

$$\int\int_T (U_t + f(U)_x)\, dx\, dt = 0.$$

From Green's theorem, we have

$$\int_T f(U)\, dt - U\, dx = 0, \tag{3.2}$$

which classically leads to the following averaged form of the conservation laws:

$$\begin{aligned} U_j^{n+1} = U_j^n - \frac{1}{h_j^n}\Bigg[& \int_{t_n}^{t_{n+1}} (f(U^*(U_{j+1}^n, U_j^n)) \\ & - V^n U^*(U_{j+1}^n, U_j^n)\Bigg)\, dt \\ & - \int_{t_n}^{t_{n+1}} (f(U^*(U_j^n, U_{j-1}^n)) - V^n U^*(U_j^n, U_{j-1}^n))\, dt. \end{aligned} \tag{3.3}$$

Here $U^*(U_L, U_R)$ is the constant value along cd or ab of the Riemann solution with initial data (U_L, U_R). If we introduce the notation:

$$\tilde{f}^n(U) = f(U) - V^n U,$$

then (3.3) takes the form:

$$\begin{aligned} U_j^{n+1} = U_j^n - \frac{k_n}{h_j^n}\,(\tilde{f}^n(U^*(U_{j+1}^n, U_j^n)) \\ - \tilde{f}^n(U^*(U_j^n, U_{j-1}^n)). \end{aligned} \tag{3.4}$$

One has to be careful when a phase boundary is being dealt with. Suppose $x_{j_0+1/2}$ is a phase boundary. Then the Riemann solution at $x_{j_0+1/2}$ in the cell j_0 is

$$U^*(U_{j_0+1}^n, U_{j_0}^n) = U^-(U_{j_0+1}^n, U_{j_0}^n)$$

and the Riemann solution at $x_{j_0+1/2}$ in cell $j_0 + 1$ is

$$U^*(U_{j_0+1}^n, U_{j_0}^n) = U^+(U_{j_0+1}^n, U_{j_0}^n)$$

(see Section 2.2 for the notation). So

$$\begin{aligned} U_{j_0}^{n+1} = U_{j_0}^n - \frac{k_n}{h_{j_0}^n}\,(\tilde{f}^n(U^-(U_{j_0+1}^n, U_{j_0}^n)) \\ - \tilde{f}^n(U^*(U_{j_0}^n, U_{j_0-1}^n)), \end{aligned} \tag{3.5}$$

$$\begin{aligned} U_{j_0+1}^{n+1} = U_{j_0+1}^n - \frac{k_n}{h_{j_0+1}^n}\,(\tilde{f}^n(U^*(U_{j_0+2}^n, U_{j_0+1}^n)) \\ - \tilde{f}^n(U^+(U_{j_0+1}^n, U_{j_0}^n)). \end{aligned} \tag{3.6}$$

We summarize the algorithm as follows:

1. Compute the speed of propagation of the phase boundary from (2.22).
2. Shift grid points according to: $x_{j+1/2}^{n+1} = x_{j+1/2}^n + V^n k^n$.
3. Compute U_j^{n+1} from (3.4).
4. Repeat steps 1–3.

Compared with shock capturing schemes, this algorithm has the following features:

- Moving grid
- Special Riemann solutions at a phase boundary.

When $V^n = 0$, this algorithm reduces to the Godunov method. When applied to conventional shock wave problems, the above algorithm is a standard Lagrangian-type method combining shock tracking and shock capturing. Several Godunov-type methods can be used to implement the above idea, The Godunov scheme, the MUSCL scheme, the PPM scheme, and the ENO scheme are some of the examples. Not every variant in each class of schemes

can be used in a straightforward manner, however. The scheme needs to be "tested" on a cell containing a phase boundary; a cell average across the phase boundary must be avoided. If this is not possible, the scheme should not be used for phase boundary problems. For instance, several schemes are based on analytically solving a linear advection equation and extrapolating the result to a general scheme for nonlinear equations; this in general would not produce the desirable property we require here—no spreading of the phase boundary. We observe that one can use a scheme in cells (I) which do not contain any phase boundary, and another scheme in cells (II) where a phase boundary is located. Such hybridization should be done carefully in order to keep the same accuracy in both regions I and II.

Schemes that can be applied include: the Godunov method (first-order method), a variant of the MUSCL scheme [52] (second-order method), and some even higher order schemes. In fact, any scheme whose numerical flux is constructed through solutions based on solving Riemann problems at cell interfaces can be used. In the numerical experiments we present in Section 6, we shall implement the Godunov method and a slope-limiter scheme.

3.2. Propagation, Initiation, and Interaction

In any computational cell, we distinguish three cases:

(i) propagation of a phase boundary,

(ii) nucleation of a phase boundary at a boundary point, or nucleation of two phase boundaries in the interior of the domain,

(iii) interaction of two phase boundaries.

The interaction between a shock wave and a phase boundary is taken care of automatically since shock waves are captured. In this subsection, we present some details of the algorithm for computing the propagation of a phase boundary. With some modification, the algorithm allows us to treat the nucleation and the interaction of phase boundaries.

3.2.1. *Propagation of a phase boundary*

One obvious shortcoming of the algorithm described in Section 3.1 is that the grid points are shifted uniformly: it cannot be applied to an initial value problem with multiple phase boundaries or an initial-boundary value problem. We are going now to shift grid points locally. As a consequence we will have a locally nonuniform mesh due to two cells moving with the phase boundary in a certain way. Assume at time t_n, $x_{j_0+1/2}$ represents a position of the phase boundary. At time t_{n+1}, $x_{j_0+1/2}$ moves to a new position. Instead of letting all grid points move with the phase boundary, we move the point $j_0 + \frac{1}{2}$ only. But subsequently

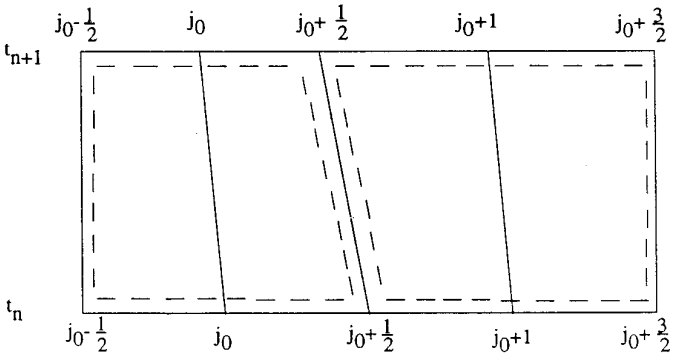

FIG. 5. Local shifting of a grid point.

the locations of j_0, $j_0 + 1$ are changed (Fig. 5). By doing this, the size of cells j_0 and $j_0 + 1$ will change as time goes on: one cell will shrink; the other will be enlarged. When one cell is too small, we adjust the location of one grid point.

The modified algorithm then reads as follows:

1. Compute U_j^{n+1} from (3.4) with $V^n = 0$ for all of the jth cell not containing the phase boundary.

2. Compute the phase boundary propagation speed V^n from the kinetic relation for the jth cell containing the phase boundary.

3. Shift grid points locally by distinguishing two cases. If $V^n < 0$:

• If $|x^n_{j_0+1/2} - x^n_{j_0+1/2}| > h/2$, then shift the point $j_0 + \frac{1}{2}$ and compute the cell averages in the cells j_0 and $j_0 + 1$ from the formulas:

$$U^{n+1}_{j_0} = \frac{h^n_{j_0}}{h^{n+1}_{j_0}} U^n_{j_0} - \frac{k_n}{h^{n+1}_{j_0}} (\tilde{f}^n(U^-(U^n_{j_0+1}, U^n_{j_0})) - \tilde{f}^n(U^*(U^n_{j_0}, U^n_{j_0-1}))$$

and

$$U^{n+1}_{j_0+1} = \frac{h^n_{j_0}}{h^{n+1}_{j_0+1}} U^n_{j_0+1} - \frac{k_n}{h^{n+1}_{j_0+1}} (\tilde{f}^n(U^*(U^n_{j_0+2}, U^n_{j_0+1})) - \tilde{f}^n(U^+(U^n_{j_0+1}, U^n_{j_0})).$$

• Otherwise adjust the location of the grid point $j_0 - \frac{1}{2}$ in the following way:

— Move the point $j_0 - \frac{1}{2}$ to the right side of the phase boundary, and relabel it as $j_0 + \frac{1}{2}$, so that the cell $[x_{j_0+1/2}, x_{j_0+3/2}]$ keeps a "regular" size of $O(h)$. Relabel the phase boundary as $j_0 - \frac{1}{2}$.

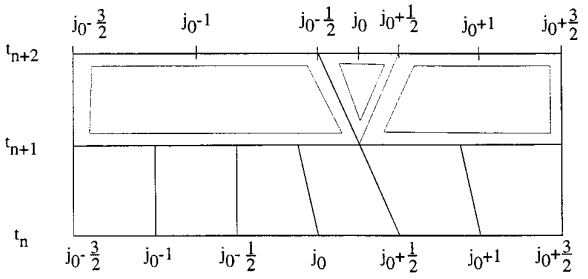

FIG. 6. Calculation of cell average for the adjusted cells.

— $j_0 - 1, j_0, j_0 + 1$ are changed accordingly for the three adjusted cells.

Then recompute the cell averages associated with the modified cells. The formulas are similar to those used in the last step. See Fig. 6.

If $V^n > 0$, the procedure is similar to that of the case $V^n < 0$:

• If $|x^n_{j_0+1/2} - x^n_{j_0+3/2}| > h/2$, then shift the point $j_0 + \frac{1}{2}$ and compute the cell averages in the cells j_0 and $j_0 + 1$.

• Otherwise modify the location of the grid point $j_0 + \frac{3}{2}$ and compute the cell averages for the adjusted cells.

4. Repeat 1–3.

It should be noted that the restriction $|ck/h| < \frac{1}{2}$ is necessary in our algorithm. This is due to the fact that computational cells can shrink as time evolves. Also a shrunken cell must be large enough, compared with h, in order to avoid local time-marching.

3.2.2. *Initiation and Interaction*

Although the above algorithm is presented for the case of a single phase boundary, it can treat multiple phase boundaries and the interaction of phase boundaries, as well. When phase boundaries are separated by, at least, one grid point (i.e., two cells), the algorithm in Section 3.2.1 can be used without modification. When two phase boundaries are too close to each other, i.e., typically when there is no grid point separating the two phase boundaries, then some modification is necessary. This is the subject of this subsection.

Since a phase boundary has to be a grid point, when a new phase nucleates, the cells near the new phase boundaries will be very small at the initial stage. In the meantime, the large difference in cell sizes may lead to computational instability. Therefore local time-marching and local mesh regridding and refinement are necessary in general. Hence we emphasize that:

(1) a phase boundary has to be a grid point.

(2) conservation of physical quantities must be preserved when local mesh regridding or local mesh refinement is carried out;

(3) local time marching must end at a regular time step.

The collision of two phase boundaries can be treated as in a method of Shyue [58] for the collision of two strong shocks. After the collision of two phase boundaries, two possible situations arise:

(a) no phase boundary comes out of the collision;

(b) two phase boundaries nucleate at the position of collision.

Case (a) is a conventional shock wave issue, and case (b) involves a nucleation problem. Both cases can be treated. The nucleation criterion presented in Section 2.2 is used for case (b).

3.3. Consistency and Entropy Condition

It would be interesting to investigate the mathematical properties of the method presented in Section 3. Questions to be addressed would include consistency, stability, the entropy condition, and strong convergence. The numerical analysis of the method is complicated by the fact that a locally nonuniform mesh is used. The main difficulty concerning convergence is to prove that the kinetic relation and nucleation criterion are satisfied by the scheme in the limit as the mesh sizes go to zero. This subsection is devoted to some preliminary investigation of the properties of our algorithm.

From (3.4), the numerical flux in the method is

$$F(U^n_{j+1}, U^n_j) = f(U^*(U^n_{j+1}, U^n_j)) - V^n U^*(U^n_{j+1}, U^n_j)$$

and, in general,

$$F(U, U) = f(U) - VU \neq f(U).$$

It might seem that the algorithm is not in conservative form, and so it might not be consistent with the conservation laws (2.5). In fact, let us recall that the mesh is being shifted as time goes on. Therefore let us rewrite the conservation laws (2.5) for coordinates moving at speed V. Let x_0 be the coordinate for fixed coordinates. Let x_0 be a point in the moving coordinates, then the coordinate of the point in the fixed coordinates is $x_0 + Vt$. We write

$$\frac{DU}{Dt} \equiv \frac{d}{dt} U(x_0 + Vt, t) = V \frac{\partial U}{\partial x} + \frac{\partial U}{\partial t},$$

so that from Eq. (2.5) we obtain

$$\frac{DU}{Dt} + \frac{\partial}{\partial x}(f(U) - VU) = 0. \tag{3.7}$$

Thus the algorithm is in fact a conservative method for Eq. (3.7), and, in view of (3.7), it is not hard to check that it is consistent; assuming that the scheme converges in the strong norm the limit must be a solution to the conservation laws (2.5).

One of the important properties of our scheme is that it is conservative across the phase boundary. This is not obvious judging from (3.5) and (3.6). This property is a consequence of the fact that the numerical fluxes on either side of the phase boundary, $\tilde{f}^{\pm}$, cancel each other:

$$\tilde{f}^n(U^+(U^n_{j_0+1}, U^n_{j_0})) - \tilde{f}^n(U^-(U^n_{j_0+1}, U^n_{j_0})) = 0.$$

The above equality holds because U^- and U^+ are Riemann solutions which satisfy the jump conditions (2.6) and (2.7).

Observe that the algorithm is a Godunov-type scheme and analytical solutions to the Riemann problems are used. These analytical solutions satisfy the entropy criterion (2.12). Therefore the algorithm is a consistent, conservative, and entropically admissible method. The Lax–Wendroff theorem then implies that the numerical solution obtained by the algorithm converges to an entropy weak solution to the conservation laws (2.5) as the mesh size approaches zero. This analysis, however, does not apply to the kinetic relation and the nucleation criterion. This part of the analysis is left for future investigation. In Section 6, we demonstrate the convergence of the algorithm numerically.

4. THE RANDOM CHOICE SCHEME

The random choice scheme was introduced by Glimm in his pioneering paper [22] as part of a constructive existence proof for systems of nonlinear hyperbolic conservation laws. In case solutions to Riemann problems of a system of conservation laws are known explicitly, the Glimm scheme can be implemented to compute the discontinuous solutions to the system. A large literature is available on the convergence of the Glimm scheme. However, only recently the case of undercompressible shock waves such as the phase boundaries received a lot of attention. The basic concepts on such waves can be found, for instance, in the recent works by Isaacson, Marchesin, and Plohr [33] and Liu and Zumbrun [44]. Stability of undercompressive waves, indeed, is an active area of research. As far as the convergence of the scheme is concerned, the first result of convergence in the case of phase boundaries was given recently by LeFloch in [41]. Therein the existence of solutions to the Abeyaratne–Knowles model is established via the Glimm scheme. Glimm's scheme is applicable and convergent for computing propagating phase boundaries.

In Glimm's original algorithm, one should shift the mesh by half a mesh size at every time step. Here we shall follow a modified algorithm proposed by Colella [15] and implement the Glimm scheme on a fixed mesh. We use the following numerical discretization. We denote by $x_{j+1/2}$ the grid points. So $[x_{j-1/2}, x_{j+1/2}]$ represents a cell, and x_j is the center of the cell, $h_j = x_{j-1/2} - x_{j+1/2}$ is the cell width. The time step is denoted by k. We denote by $R^n_{j-1/2}$ the Riemann solution at the point x_{j-1} and the time nk. Set also:

$$\hat{U}^n_{j-1/2} = R^n_{j-1/2}\left(\left(a^{n+1} - \frac{1}{2}\right)\frac{h}{k}\right). \tag{4.1}$$

Given the approximate solution $\{U^n_j\}_j$ at time t_n, Glimm scheme is composed of the following main two steps:

(i) Solve the Riemann problems at the cell interfaces $x_{j-1/2}$ with initial data (U^n_{j-1}, U^n_j) $(j = ..., -1, 0, 1, ...)$. The solution at the time $t = t_{n+1}$ is known for every x.

(ii) $\{U^{n+1}_j\}_j$ is determined by sampling according to the following formula:

$$U^{n+1}_j = \begin{cases} \hat{U}^n_{j-1/2}, a^{n+1} > \frac{1}{2}, \\ \hat{U}^n_{j+1/2}, a^{n+1} < \frac{1}{2}. \end{cases} \tag{4.2}$$

Here $\{a^n\}$ is a given random sampling sequence in (0, 1). So, in Glimm's scheme, one chooses a point value of a local exact solution for $\{U^{n+1}_j\}_j$, instead of a cell average in Godunov's method.

5. EXTENSION TO MORE GENERAL MATERIALS

Our front tracking/capturing method in principle can be applied to any material, although we so far only present the method for trilinear materials. Of course, it is of both theoretical and practical interest to apply the method to general two-phase materials; see Fig. 7. We assume that the stress–strain relation of these materials satisfies

$$\sigma'(\gamma) \geq 0 \quad \text{for } -1 < \gamma \leq \gamma_m,$$

$$\sigma'(\gamma) < 0 \quad \text{for } \gamma_m < \gamma \leq \gamma_M,$$

and

$$\sigma'(\gamma) \geq 0 \quad \text{for } \gamma_M < \gamma.$$

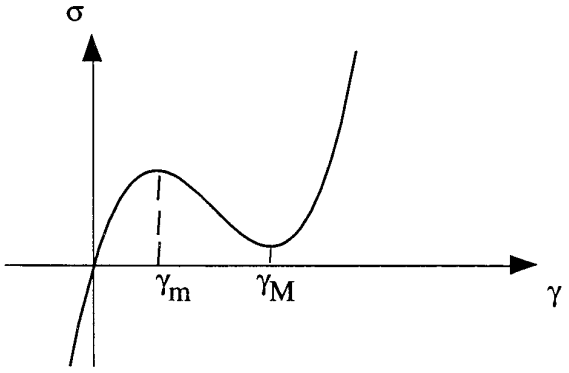

FIG. 7. A nontrilinear two-phase elastic material.

We observe that explicit analytical Riemann solutions for a general two-phase elastic material capable of phase transitions are not easily available. Solving Riemann problems is done numerically by an iterative method for nonlinear algebraic equations. In practice, this is time-consuming and the convergence of the iteration method cannot be always guaranteed because we cannot always have a good initial guess of the solutions. Motivated by Roe's scheme in the computation of shock waves, an approximate Riemann solver is proposed by Zhong [65]. We shall follow the basic idea of Roe [53]. The main idea is to determine Riemann solutions by solving a constant coefficient linear system of conservation laws instead of the original nonlinear system. For the conservation laws (2.5), we consider the approximation:

$$\nabla f(U) = \begin{pmatrix} 0 & -\dfrac{\sigma'(\gamma)}{\rho} \\ -1 & 0 \end{pmatrix} \approx \begin{pmatrix} 0 & -c^2 \\ -1 & 0 \end{pmatrix} = A.$$

Here c is a constant to be determined. For definiteness, we consider 3–1 initial data only, that is, data: $U_l = (v_l, \gamma_l)$, $U_r = (v_r, \gamma_r)$ with γ_l, γ_r in high strain phase (phase 3) and low strain phase (phase 1), respectively. The algorithm for the approximate Riemann solver reads as follows:

1. Set $c_l = (\sigma'(\gamma_l)/\rho)^{1/2}$ and $c_r = (\sigma'(\gamma_r)/\rho)^{1/2}$. Then we approximate the general stress–strain relationship $\sigma(\gamma)$ by the trilinear stress–strain relation

$$\hat{\sigma}(\gamma) = \begin{cases} \rho c_r^2(\gamma - \gamma_r) + \sigma(\gamma_r), & -1 < \gamma < \gamma_m, \\ \dfrac{\hat{\sigma}_m - \sigma_M}{\gamma_m - \gamma_M}(\gamma - \gamma_M) + \hat{\sigma}_M, & \gamma_m < \gamma < \gamma_M, \\ \rho c_l^2(\gamma - \gamma_l) + \sigma(\gamma_l), & \gamma_M < \infty, \end{cases} \tag{5.1}$$

where $\hat{\sigma}_m = \rho c_r^2 (\gamma_m - \gamma_r) + \sigma(\gamma_r)$ and $\hat{\sigma}_M = \rho c_l^2 (\gamma_M - \gamma_l) + \sigma(\gamma_l)$. Solve the conservation laws for the trilinear material for the U_-^1, U_+^1 which are U right behind and in front of the phase boundary. The phase boundary propagation speed $\dot{s}_1$ is determined by the kinetic relation.

2. From the conservative requirement in hyperbolic regions, we improve the linear coefficient matrix A in the following way:

$$f(U_l) - f(U_-^n) = \hat{A}_l(U_l - U_-^n),$$
$$f(U_r) - f(U_+^n) = \hat{A}_r(U_r - U_+^n).$$

From these conditions, we have

$$c_l = \left(\frac{\sigma(\gamma_l) - \sigma(\gamma_-^n)}{\rho(\gamma_l - \gamma_-^n)}\right)^{1/2} \tag{5.2}$$

and

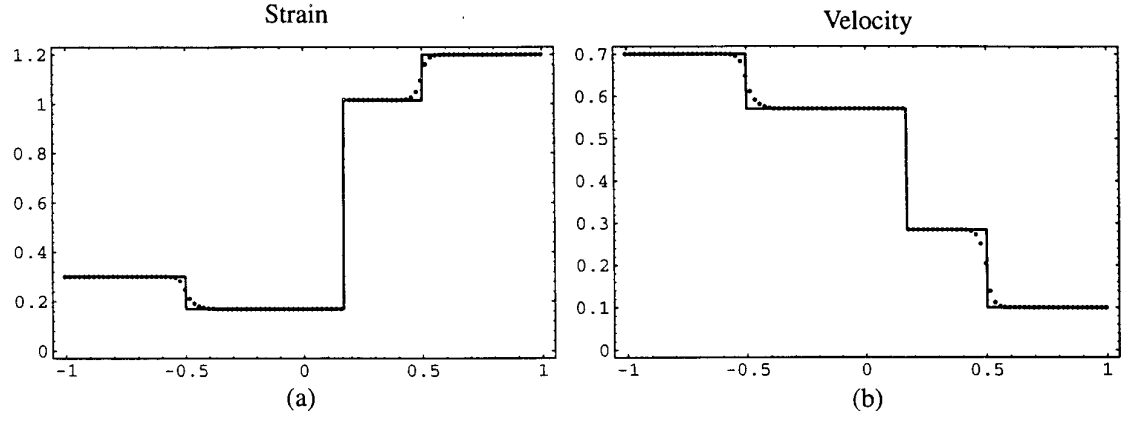

FIG. 8. Solutions to Riemann problem with 1–3 initial data at $t = 0.5$ by front tracking: (a) the strain distribution; (b) the velocity distribution.

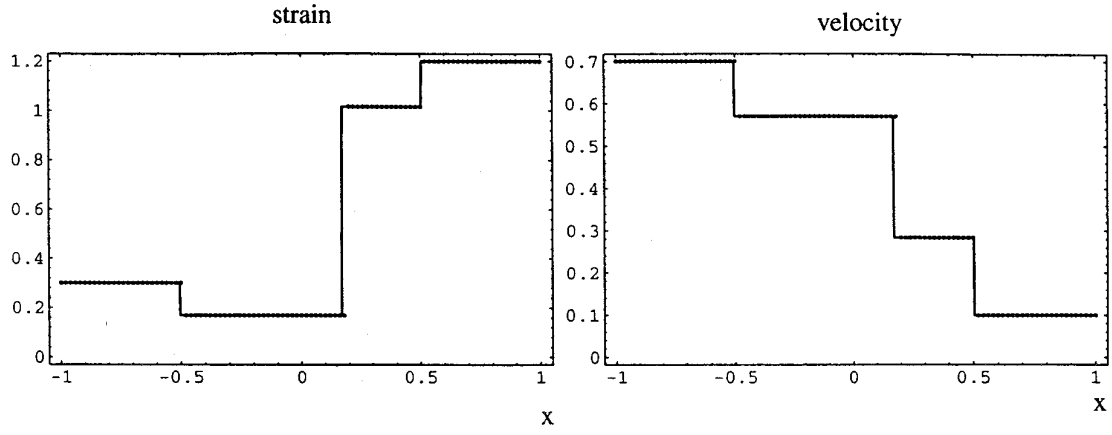

FIG. 9. Solutions to Riemann problem with 1–3 initial data at $t = 0.5$ by Glimm's scheme: (a) the strain distribution; (b) the velocity distribution.

$$c_r = \left(\frac{\sigma(\gamma_r) - \sigma(\gamma_+^n)}{\rho(\gamma_l - \gamma_+^n)} \right)^{1/2}. \tag{5.3}$$

Then we approximate the general stress–strain relationship $\sigma(\gamma)$ by an improved trilinear stress–strain relation which has the same form as that in Step 1. We solve the new approximate conservation laws for the new trilinear stress–strain relation for U_-^{n+1} and U_+^{n+1} which are the values of U right behind and in front of the phase boundary. The phase boundary propagation speed $\dot{s}_n$ is determined by the kinetic relation.

3. If $|\dot{s}_n - \dot{s}_{n-1}| < \varepsilon$ (where ε is given small enough), then we get the following approximate solutions: $\dot{s} = \dot{s}_n$, $U_- = U_-^n$, $U_+ = U_+^n$. The solution is illustrated in Fig. 1.

4. If $\sigma'(\gamma_l) > \sigma'(\gamma_-)$, we replace the left shock by a rarefaction wave in $-(\sigma'(\gamma_l)/\rho)^{1/2} < x/t < -(\sigma'(\gamma_-)/\rho)^{1/2}$. If $\sigma(\gamma_r) > \sigma'(\gamma_+)$, we replace the right shock by a rarefaction wave in $(\sigma'(\gamma_+)/\rho)^{1/2} < x/t < (\sigma'(\gamma_r)/\rho)^{1/2}$.

It can be easily checked that the above algorithm satisfies in the hyperbolic regions the three conditions on the linearization as suggested by Roe in [53]. As the phase boundary is not known a priori, the above ''linearized version'' of the conservation laws are still nonlinear. We apply the approximate Riemann solver to two 3–1 initial data Riemann problems for the hypothetical nontrilinear stress–strain relation constructed in [65]:

$$\sigma(\gamma) = \begin{cases} -\dfrac{0.0071}{1+\gamma} + 14.64\gamma - 0.953 & \text{for } -1 < \gamma < -0.9, \\ \gamma(\gamma^2 - 4.4\gamma + 5) & \text{for } -0.9 \le \gamma < 4, \\ \dfrac{950}{1+\gamma} + 55.8\gamma - 399.8 & \text{for } 4 \le \gamma < \infty. \end{cases} \tag{5.4}$$

We have here: $\gamma_m = 0.770646$ and $\gamma_M = 2.1629$. This stress–strain relation corresponds to a material model proposed by Lin [43].

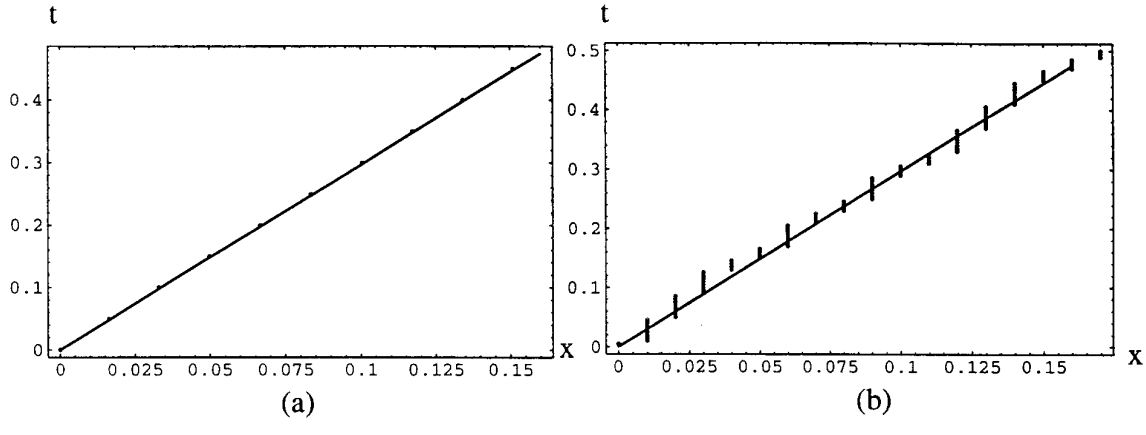

FIG. 10. Trajectory of the phase boundary determined by (a) front-tracking method; (b) Glimm's scheme.

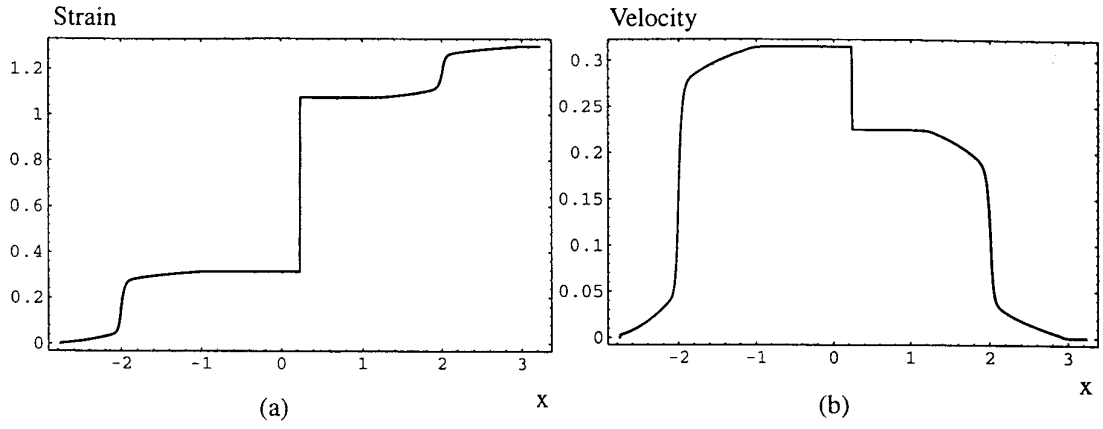

FIG. 11. Solutions to Riemann problem with 1–3 initial data at $t = 2$ by front-tracking: (a) the strain distribution; (b) the velocity distribution.

Let us consider two examples:

Test 1: 1-shock, 1-subsonic phase boundary, 1-shock ($\rho = 1$) obtained from the initial condition: $(v_l, g_l, v_r, g_r) = (0, 2.5, -0.5, 0.5)$ and $\omega = 0.5$.

Methods	Approximate Riemann solver	Exact Riemann solver
$\dot{s}$	−0.14070	−0.15547
v_+	−0.10279	−0.11767
γ_+	0.23198	0.24046
v_-	0.23859	0.26024
γ_-	2.65840	2.67122

Test 2: 1-shock, 1 subsonic phase boundary, 1-rarefaction wave ($\rho = 1$) obtained from the initial condition: $(v_l, g_l, v_r, g_r) = (-1.6, 2.7, 0.1, 0.1)$ and $\omega = 0.5$.

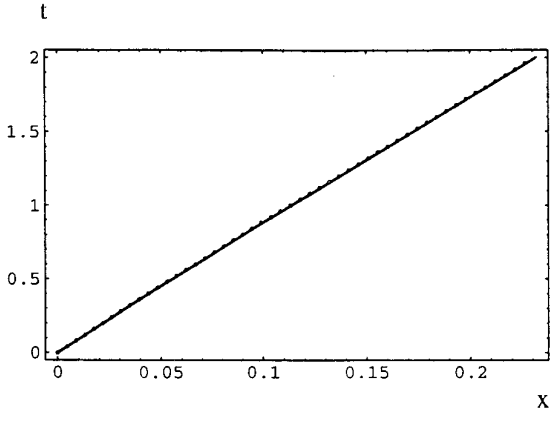

FIG. 12. Trajectory of the phase boundary determined by front-tracking method.

Methods	Approximate Riemann solver	Exact Riemann solver
$\dot{s}$	0.49437	0.51091
v_+	−0.10773	0.06913
γ_+	0.20767	0.18677
v_-	−1.39407	−1.40610
γ_-	2.80966	2.80359

By an "exact" Riemann solver, we mean a procedure to obtain the Riemann solutions directly from the original set of nonlinear equations and their jump conditions using Newton iterations. For further discussion on the structure of the solution to Riemann problem for general two-phase elastic materials, one refers to [43, 65]. From the two tests, we see that the approximate Riemann solver works reasonably well. On the other hand, we note that the discrepancy between the numerical solution based on the approximate Riemann solver and that of the exact one will not go to zero as we refine the mesh (see Test 7). Therefore if we use such an approximate Riemann solver in our numerical scheme, it would not give a convergent method. In order to obtain a convergent scheme based on the approximate Riemann solver, we propose to use the above Riemann solver, together with a nonlinear Newton iterative method. We will use the above Riemann solver to produce an accurate initial guess and use it in our nonlinear Newton iteration scheme. This proves to be very effective. The Newton iterations typically converge to the correct Riemann solution with only a few iterations (2 or 3).

The above approximate Riemann solver can be applied to our front tracking/capturing method. Following the general procedure in Section 3.1, we obtain the following approximate flux at a phase boundary that is propagating with the speed V,

$$\tilde{f}(U_l, U_r) = A\hat{U}^* - V\hat{U}^* + f(U_r) - AU_r, \qquad (5.5)$$

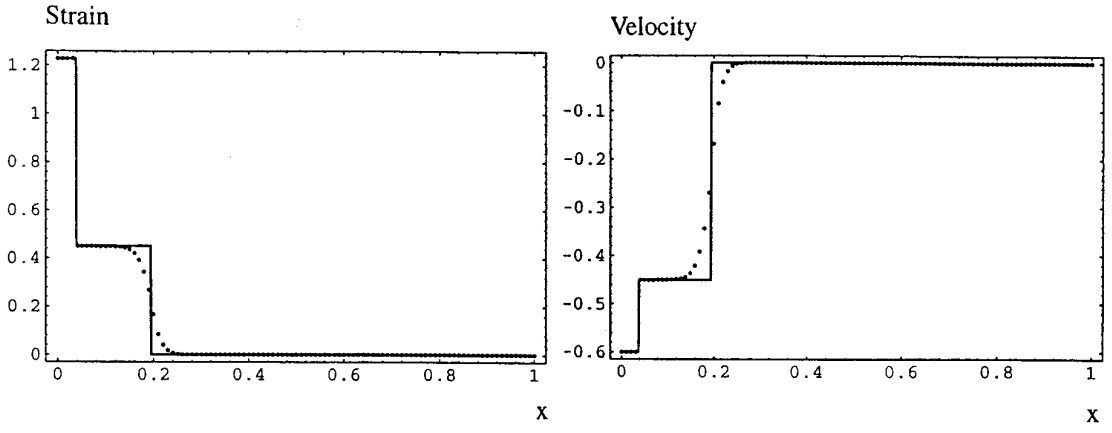

FIG. 13. Solutions to the problem involving nucleation of a phase boundary by front tracking at $t = 0.2$: (a) the strain distribution; (b) the particle velocity distribution.

where $\hat{U}^*$ is the approximate Riemann solution at the phase boundary. Fluxes away from a phase boundary can be computed by the classical Roe's approximate Riemann solver, and the corresponding approximate flux is obtained. We emphasize that the conservation of U is guaranteed by Roe's approach. On the other hand, the propagation of a phase boundary is determined by simply using the above flux into the algorithm in Section 3.2. Using an approximate Riemann solver, we can compute propagation of phase boundaries associated with general two-phase elastic materials.

6. NUMERICAL EXPERIMENTS

We implement the front tracking/capturing method by Godunov scheme and a slope-limiter scheme, which is equivalent to a variant of the MUSCL scheme [52]. It should be pointed out that the slope-limiter in the MUSCL scheme, based on the so-called minmod limiter in our code, is determined unilaterally instead of bilaterally by minmod when a phase boundary is present in a cell. In Tests 1–6, the material is the trilinear material defined in Section 2. The kinetic relation is given by $f = \omega\dot{s}$. The material constants are: $\mu = 1$, $\rho = 1$, $\omega = 0.35$, $\gamma_m = 0.5$, $\gamma_M = 1.0$, $\gamma_T = 0.75$, $\gamma_{\rm cr} = 0.5$, $\gamma^*_{\rm cr} = 1.0$. In the computations, the time step is 0.001 (time unit), the mesh size h is 0.01 (length unit), if not otherwise specified. In applicable diagrams, the analytical solutions are represented by solid lines, numerical solutions are represented by dashed lines or dots. An equidistributed sequence $a_n = n\sqrt{2} - [n\sqrt{2}]$ is used in the computation of Glimm scheme. Here $[n\sqrt{2}]$ represents the integer part of $n\sqrt{2}$.

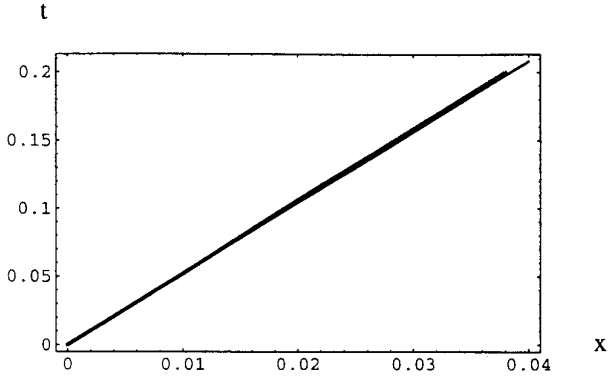

FIG. 14. Trajectory of the phase boundary.

More specifically, we compute the propagation of a single phase boundary in Test 1. We also check the convergence of our method in this test numerically. In the convergence test, we find that the Godunov scheme implemented in our method is of order $O(h^{0.5})$ in the discrete L^1 norm, rather than $O(h)$. This is because in the trilinear materials the shock waves degenerate to contact discontinuities. The spreading of the discontinuity is of order $(O(\sqrt{h})$. For real shocks, we expect that the Godunov scheme is of order $O(h)$; see more discussions on this in Test 7. Numerical results of an initial value problem with complex initial data are presented in Test 2. The results show that our scheme can deliver accurate results for complicated cases. Nucleation of new phase and collision of two phase boundaries are computed in Tests 3–5. The improvement of accuracy of the computed phase boundary position is obtained with local mesh refinement. In Test 6, a much more complicated problem is considered, which involves the interaction of the phase boundary with shock waves. The numerical solution generated by our front tracking/capturing method is in very good agreement with the analytical solution. The propagation of a phase boundary in a finite bar is

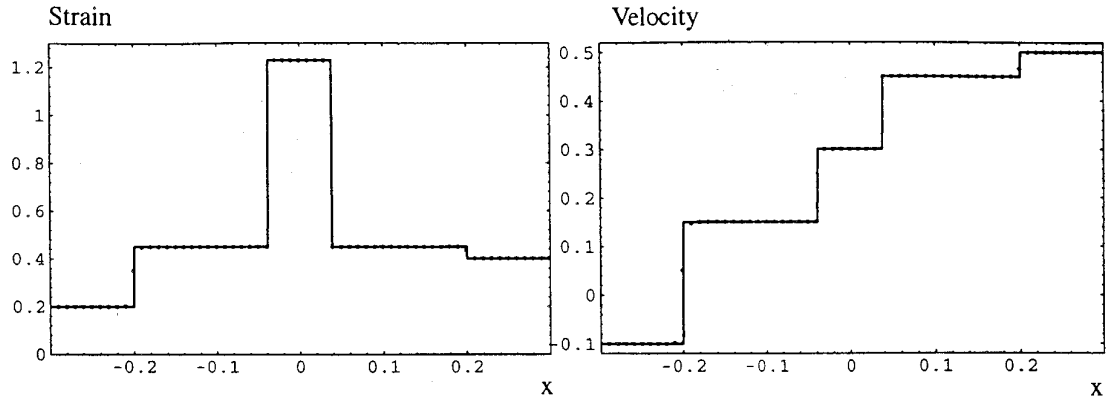

FIG. 15. Solutions to the problem involving nucleation of two phase boundaries by front tracking at $t = 0.2$: (a) the strain distribution; (b) the particle velocity distribution.

computed in Test 7. A preliminary result on general two-phase elastic materials is presented in Test 8, with more discussions on convergence.

6.1. Test 1: Single Phase Boundary

A 1–3 initial data Riemann problem is treated here. The initial data are $v_L = 0.7$, $\gamma_L = 0.3$, $v_R = 0.1$, $\gamma_R = 1.2$. We compute the propagation of a phase boundary by our tracking/capturing method and Glimm's scheme. The numerical results are compared with the exact solution that is known from Section 2.2. See Figs. 8–10. The results from the front tracking/capturing method are obtained using a slope-limiter scheme. The convergence of the front tracking/capturing method is demonstrated in the following table, where the error e is measured by l_1-norm for particle velocity or strain,

Mesh size	e (Godunov scheme)	e (slope-limiter scheme)
$2h$	1.62×10^{-2}	7.73×10^{-3}
h	1.15×10^{-2}	4.91×10^{-3}
$h/2$	8.15×10^{-3}	3.15×10^{-3}

where $h = 0.01$, $CFL = 0.1$ (fixed), $t = 0.5$. In this particular test, the errors for particle velocity and strain are about the same, so in the above table, we list only one error for each scheme.

The results show that the front tracking/capturing method converges to the exact solution when the mesh size reduces to zero, but the Godunov scheme converges at the order $O(h^{0.5})$, the slope-limiter scheme converges approximately at the order $O(h^{0.65})$. These convergence rates can be partly explained by the fact that the "shocks" in the trilinear materials are in fact contact discontinuities. As the contact discontinuities are captured in our tracking/capturing method, they are smeared out by numerical viscosity. Glimm's scheme computes sharp contact discontinuities. On the other hand, the front tracking/capturing method tracks the location of the phase boundary accurately while the trajectory of the phase boundary computed by Glimm's scheme randomly oscillates around the exact trajectory.

6.2. Test 2: Single Phase Boundary with Piecewise Smooth Initial Data

An initial value problem that associates with a single phase boundary is considered here. The initial data are,

$$v(x,0), \gamma(x,0) = \begin{cases} 0,0, & x < -1, \\ 0, 0.1(x+1)^2, & -1 < x < 0, \\ 0, 1.2 + 0.1\sqrt{x}, & 0 < x < 1, \\ 0, 1.3, & 1 < x. \end{cases}$$

It is obvious that the $x < 0$ part is in phase 1 while the $x > 0$ part is in phase 3. The initial data are continuous except at $x = 0$.

The exact solution for the initial value problem is not easy to obtain. However, we can use the method of characteristics to obtain a solution by an iterative procedure. The solution procedure is presented in the Appendix. We call solutions obtained from this procedure "the exact solution" in this test. The numerical solutions are presented in Figs. 11 and 12. Figure 12 indicates that the phase boundary propagation speed is very accurate. In this test, we fixed CFL, with $CFL = 0.1$, and take $h = 0.01$. Denote by S the distance that the phase boundary has moved from its original position at time $t = 2$. The accuracy of the phase boundary position under different mesh size is listed in the following table:

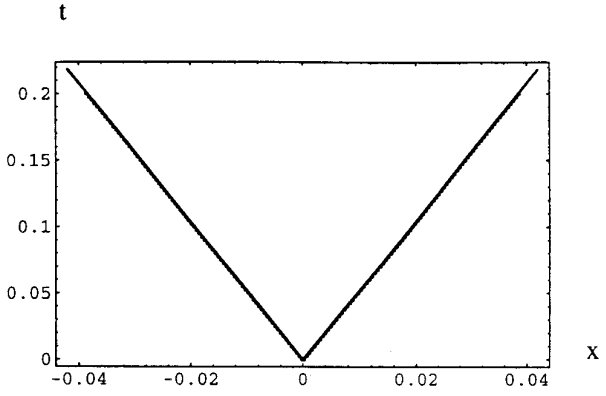

FIG. 16. Trajectories of phase boundaries.

Mesh size	$\lvert(S_{\text{exact}} - S_{\text{Numerical}})/S_{\text{exact}}\rvert$
$2h$	0.47%
h	0.24%
$h/2$	0.11%

We clearly observe a first-order convergence in the phase boundary position as we refine the mesh. It should be noted that the trajectory of the phase boundary in this case is not a straight line, but a curve with a small curvature.

6.3. Test 3: Nucleation of a Phase Boundary at an End Point

Nucleation of a phase boundary at the boundary of a bar is quite common, such as the case in bar impact experiments. In this test we only consider a very simple situation; a semi-infinite bar, which is in an initially undeformed state, is impacted at the end $x = 0$ at time $t = 0$. The boundary condition here can be described by $v(0, t) = v_{\text{b}}$, where v_b is a constant. The initial state of the bar is $v(x, 0) = 0, \gamma(x, 0) = 0$. In order to initiate a phase boundary at the boundary of the bar, the magnitude of v_b has to be large enough, $|v_b| > c\gamma_{\text{cr}}$. In this calculation, we take $v_b = -0.6$ so that we can have a nucleation at the boundary. In a real computation, at the first several time steps, the nucleated phase boundary is very close the boundary of the bar, so local time marching is necessary. After the first time step we relocate the first grid point to the phase boundary. We do local time marching in the two cells that contain the phase boundary until it is $1\frac{1}{2}$ cell away from the boundary of the bar. We continue the computation by the algorithm in Section 3.2.1. It should be noted that time step in the local time marching is adjusted according to the size of the first cell. The smallest time step in the local time marching is about $\frac{1}{12}$ of the normal time step, and the local time marching lasts 10 normal time steps. Our numerical results are in good agreement with the exact solution; see Figs. 13 and 14. Again, the front tracking/capturing method tracks the phase boundary accurately, while the contact discontinuity is smeared numerically, the error of phase boundary position is 1.15%.

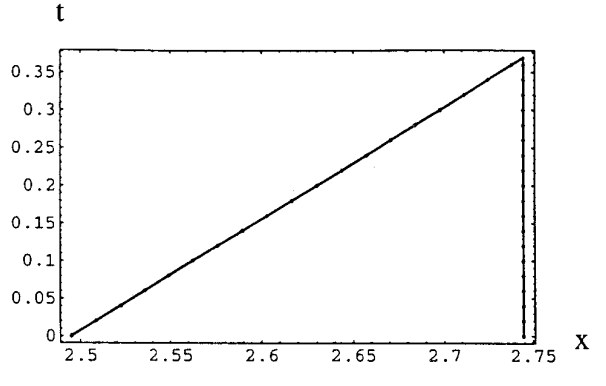

FIG. 17. Trajectories of phase boundaries for the problem involving collision of phase boundaries.

6.4. Test 4: Nucleation of Two Phase Boundaries

Due to the interaction of shock waves, a new phase may be initiated in the interior of the domain so that two phase boundaries will be generated from a single grid point. For the regridding of cells around the new phase, we can proceed as in Test 2; then we proceed by local time marching until the distance between the two new phase boundaries is no less than twice the regular cell size. However, this mesh technique does not work sometimes because the big difference of mesh sizes may produce errors that lead to numerical instability. This suggests that local mesh refinement is necessary.

We consider the nucleation of two phase boundaries in a 1–1 initial data Riemann problem. The initial data is taken to be: $v_L = -0.1$, γL $= 0.2$, $v_R = 0.5$, $\gamma_R = 0.4$. In the computation the mesh size in the refined region is $\frac{1}{10}$ of regular size, the smallest time step in local time marching is $\frac{1}{10}$ of regular time step. The numerical results are compared with analytical results in Figs. 15 and 16.

6.5. Test 5: Collision of Two Phase Boundaries

We construct special initial data which give rise to two phase boundaries colliding at a finite time. The initial data are piecewise constant in three regions that we refer to as L, C, and R. We choose: $v_L = 0.789$, $\gamma_L = -0.4$, $v_C = 0.$, $\gamma_C = 1.125$, $v_R = 0.$, $\gamma_R = 0.375$.

When two phase boundaries are so close to each other that there are no grid points in between, we treat the three cells which contain the phase boundaries as a group with no further regridding in these cells. After the interaction, the whole domain under consideration is in phase 1. Com-

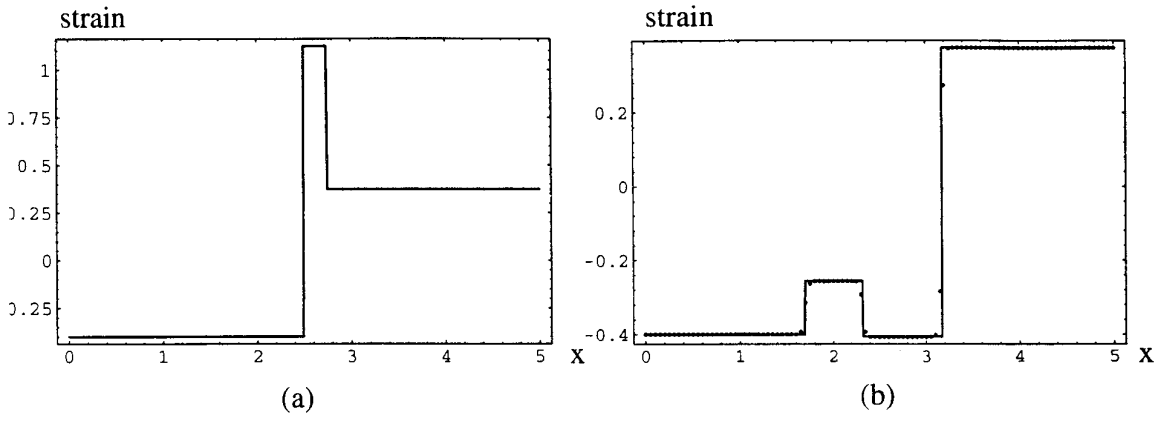

FIG. 18. The strain distribution: (a) initial strain; (b) strain after collision, $t = 0.8$.

parison between the numerical results and analytical results are given in Figs. 17–19.

6.6. Test 5: Impact on a Semi-infinite Bar with an Initially Stationary Phase Boundary

In this example, we consider the effect of impact on a semi-infinite bar initially in a two-phase equilibrium state, with a single stationary phase boundary. There is an analytical solution to this problem derived by Zhong [65]. We compare the computed phase boundary position to that of the exact solution.

A semi-infinite bar is located at $[0, \infty)$ in the reference state, and a phase boundary is initially located at $x = 1.995$, in the equilibrium state. The strains in the bar are $\gamma = 0.375$, $v = 0$ for x in $[0, 1.995)$ and $\gamma = 1.125$, $v = 0$ for x in $(1.995, \infty)$. At time $t = 0$, the bar is loaded by a velocity whose time-history is a given square wave. The duration of the square wave is 0.5 (time unit), the amplitude of the square wave is 0.15 (length unit/time unit). The numerical results are shown in Figs. 20–22. When compared with the exact solution, the position of the phase boundary as calculated numerically is accurate. For fixed CFL, we check the convergence by changing the mesh size and the time step with $h = 0.01$, $CFL = 0.1$ and S is the distance that the phase boundary has moved from its original position at time $t = 3$:

Mesh size	$\lvert(S_{\text{exact}} - S_{\text{Numerical}})/S_{\text{exact}}\rvert$
$2h$	2.45%
h	1.58%
$h/2$	0.84%

These results suggest that the numerical solution converges to the exact solution as the mesh size goes to zero. Roughly speaking the accuracy of the method is of order $O(h^2 + k)$ when a slope-limiter scheme is implemented. The improvement of the accuracy in space can be easily implemented, but improvement of the accuracy in time integration requires some changes in the formulation of the algorithm (3.4) due to the nonuniformity of the mesh.

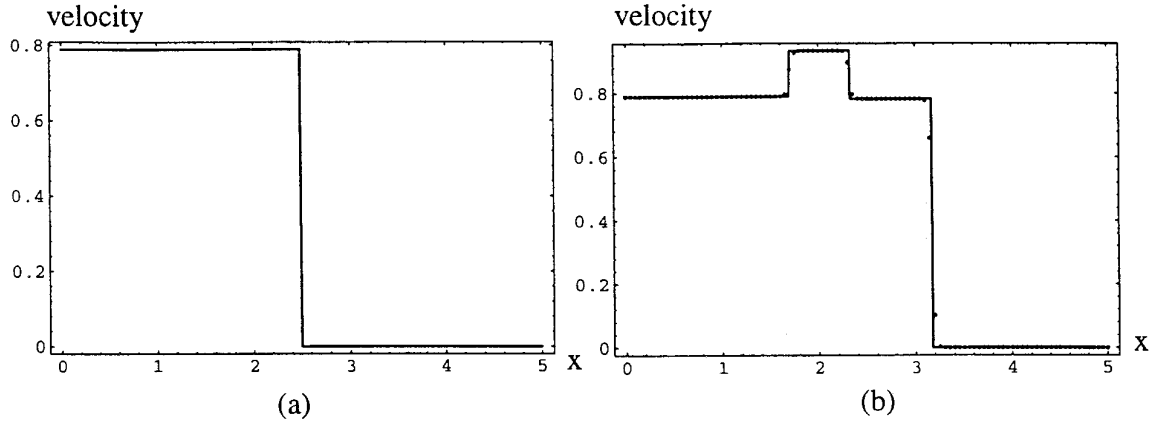

FIG. 19. The particle velocity distribution: (a) initial state; (b) velocity after collision, $t = 0.8$.

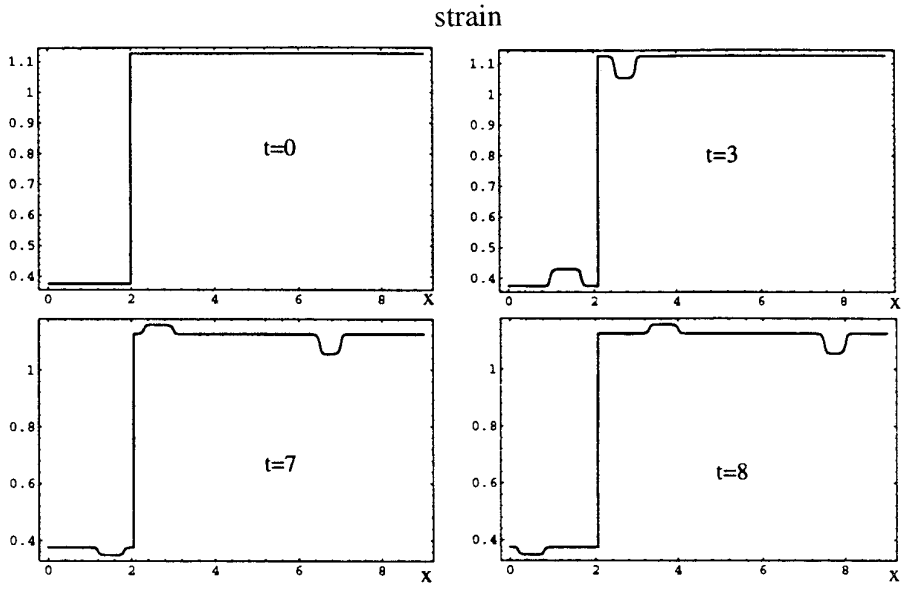

FIG. 20. The strain distribution in a semiinfinite bar at different time.

As before, the contact discontinuities are smeared out slightly. This contributes to the error in the speed of propagation of the phase boundary and, thus, in the position of the phase boundary. In the computation, the boundary values are carefully chosen so that there is no other phase boundary nucleated at any time in the bar. Glimm's scheme is also applied to the problem. However, Glimm's scheme produces a relatively large error due to the statistical errors in the random sequence. Again Glimm's scheme gives a sharp phase boundary, as well as sharp contact discontinuities; see Figs. 23 and 24.

6.7. Test 7: Propagation of a Phase Boundary in a Finite Bar

There is no analytical solutions for this case. The finite bar is located at $[0,3]$ in the reference state. A phase boundary in the bar is initially located at $x = 1.005$, with $[0, 1.005)$ in phase

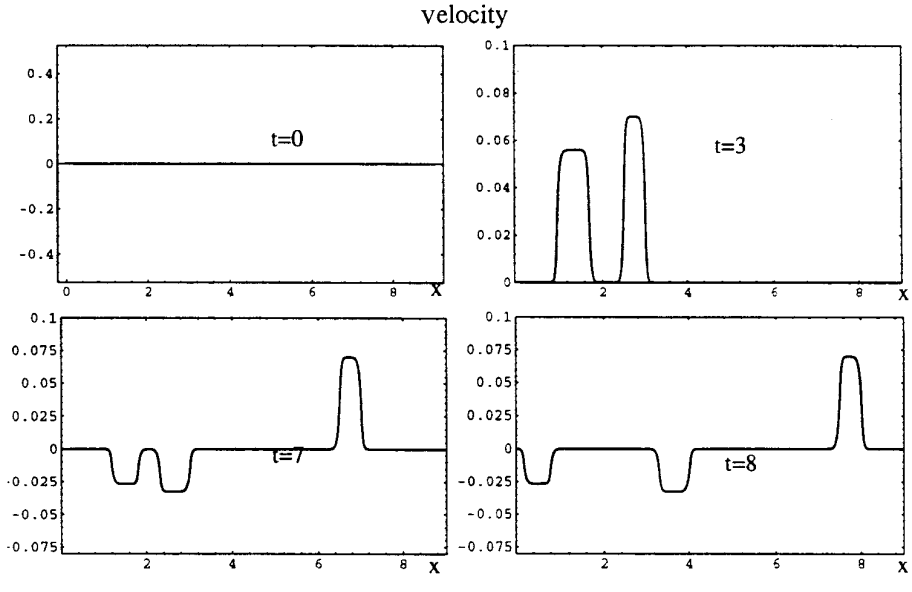

FIG. 21. The particle velocity velocity distribution in semiinfinite bar at different time.

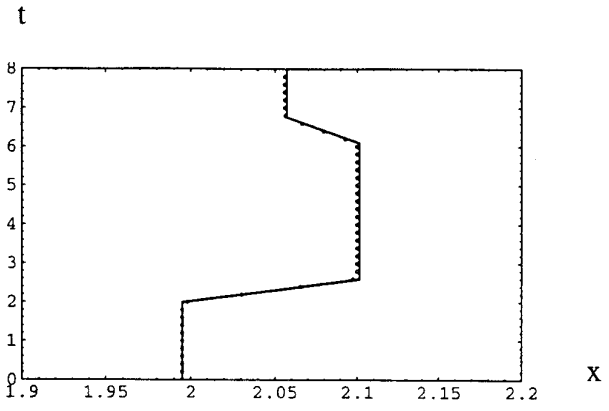

FIG. 22. Trajectory of the phase boundary determined by front tracking.

1, $\gamma = 0.375$, $v = 0$, (1.005, 3] in phase 3, $\gamma = 1.125$, $v = 0$. An impact is loaded at $x = 0$ at time $t = 0$. The load is the same as that in Test 5. The duration of the square wave is 0.5 (time unit), the amplitude of the square wave is 0.15 (length unit/time unit). The results are shown in Figs. 25–27.

In Fig. 27, as we can see, before the reflected shock wave from $x = 3$ hits the phase boundary, the phase boundary behaves as if it were in a semi-infinite bar. After the reflected waves from end point $x = 3$ hit the phase boundary, the boundary behaves quite irregularly. As time increase, there are more and more waves with smaller and smaller amplitudes in the bar. The decrease of the amplitudes is due to the dissipation of energy at the phase boundary.

Although the phase boundary will eventually reach an equilibrium state, but it takes a very long time to reach the equilibrium. And it is of theoretical interest to see whether the dynamic solution approaches corresponding static solution in large time. It has been shown numerically, for a sufficiently small loading, that the dynamic solution indeed approaches a corresponding static solution; see [65] for details about this. It should be noted that when the loading is small enough there is no new phase boundary initiated in the whole process.

6.8. Test 8: An Example for General Two-Phase Elastic Materials

We use our front tracking method and the proposed approximate Riemann solver to compute the problem involved in Test 1 and Test 2 of Section 5. A first-order Godunov scheme is used in the implementation. The results for the two tests show that our front tracking method works well when an approximate Riemann solver is used. Here we only present the results for Test 1 of Section 5; see Figs. 28, 29. The error in the computed phase boundary position is 3.81% for $h = 0.01$. For fixed mesh size, the error decreases slowly with the decrease of the time step, 3.80% for time step 0.001/2; 3.79% for time step 0.001/4. For fixed CFL, the decrease in mesh size does not improve the accuracy of computation. This ''locking'' of accuracy is due to the inherent error of the approximate Riemann solver. To remedy the deficiency, we propose the following procedure: use the Riemann solutions from the approximate Riemann solver as initial guesses for the iterative exact Riemann solver; use the Riemann solutions of the iterative exact Riemann solver to construct the numerical flux. It only takes one or two iterations for the iterative exact Riemann solver to converge when using the approximate Riemann solution as the initial guess. Using this procedure, we obtain the following convergent results:

Mesh size	$\lvert(S_{\text{exact}} - S_{\text{Numerical}})/S_{\text{exact}}\rvert$
$2h$	0.753%
h	0.479%
$h/2$	0.283%
$h/4$	0.154%

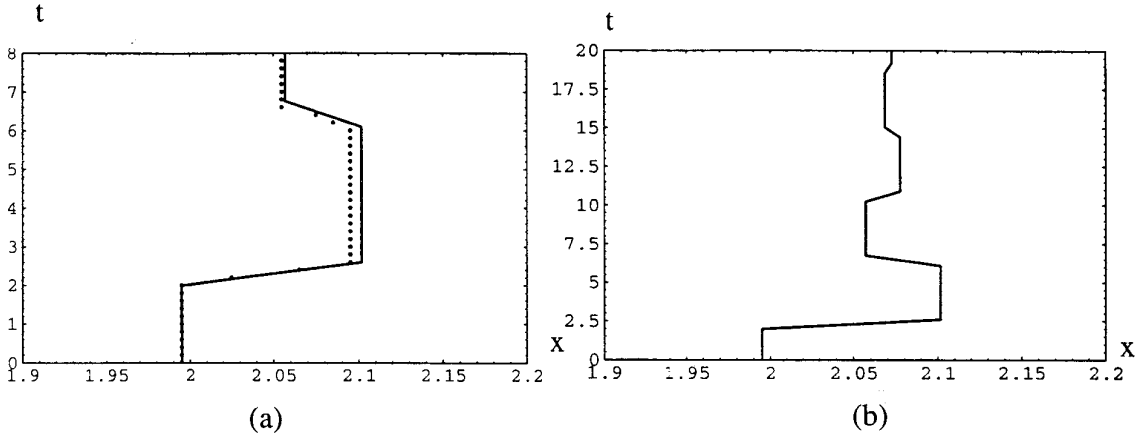

FIG. 23. Trajectory of the phase boundary determined by (a) Glimm's scheme; (b) analytical solution.

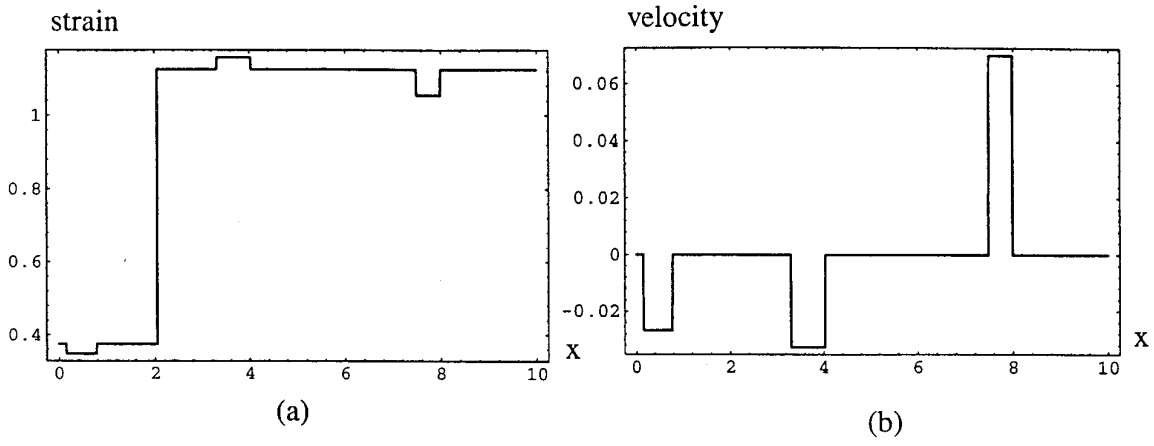

FIG. 24. Solutions to the semiinfinite bar problem by Glimm's scheme at $t = 8$: (a) the strain distribution; (b) the particle velocity distribution.

Mesh size	$e1$ (velocity)	$e2$ (strain)
$2h$	2.72×10^{-2}	1.816×10^{-2}
h	1.712×10^{-2}	1.157×10^{-3}
$h/2$	1.014×10^{-2}	6.724×10^{-3}
$h/4$	5.652×10^{-3}	3.748×10^{-3}

where $h = 0.01$, $CFL = 0.1$ (fixed), and $x = S$ is the position of the phase boundary at time $t = 0.2$. Here $e1$ and $e2$ are errors of the particle velocity and strain measured by the l_1-norm. If we compared these results with those obtained from the Godunov scheme in Test 1, we can see that the results obtained here converge at a higher order. A smaller mesh size gives a higher convergent rate. The order increased roughly from $O(h^{0.65})$ $(2h \to h)$ to $O(h^{0.85})$ $(h/2 \to h/4)$. This observation is consistent with the error analysis for the Godunov scheme; for a contact discontinuity, the Godunov scheme is of order $O(h^{0.5})$; for a shock wave, the accuracy order of Godunov scheme should approach $O(h)$ as mesh size goes to zero.

7. CONCLUDING REMARKS

Our tests demonstrate that the tracking/capturing method can treat initial-boundary value problems in the modeling of solid–solid phase transformations. The

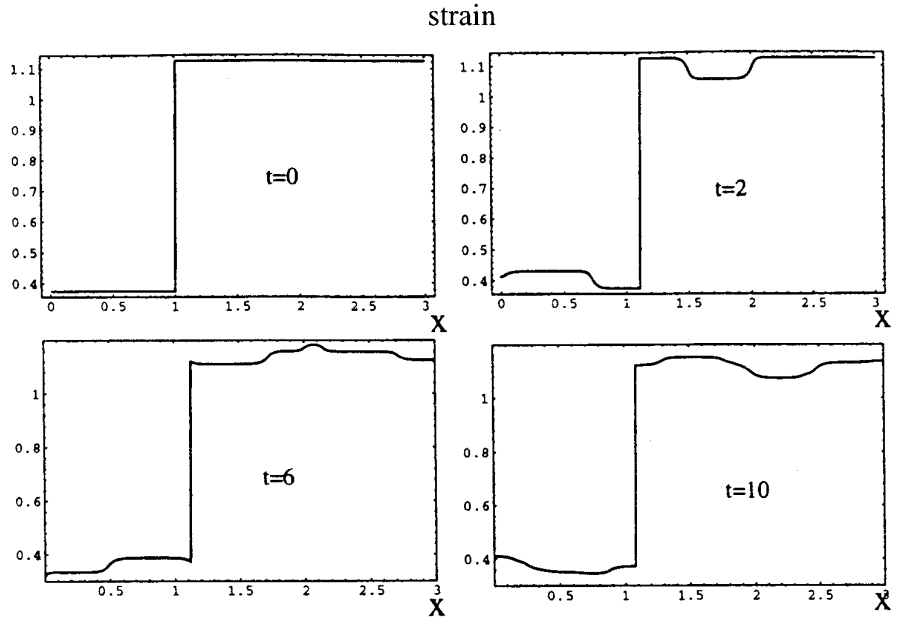

FIG. 25. The strain distribution in a finite bar at different time.

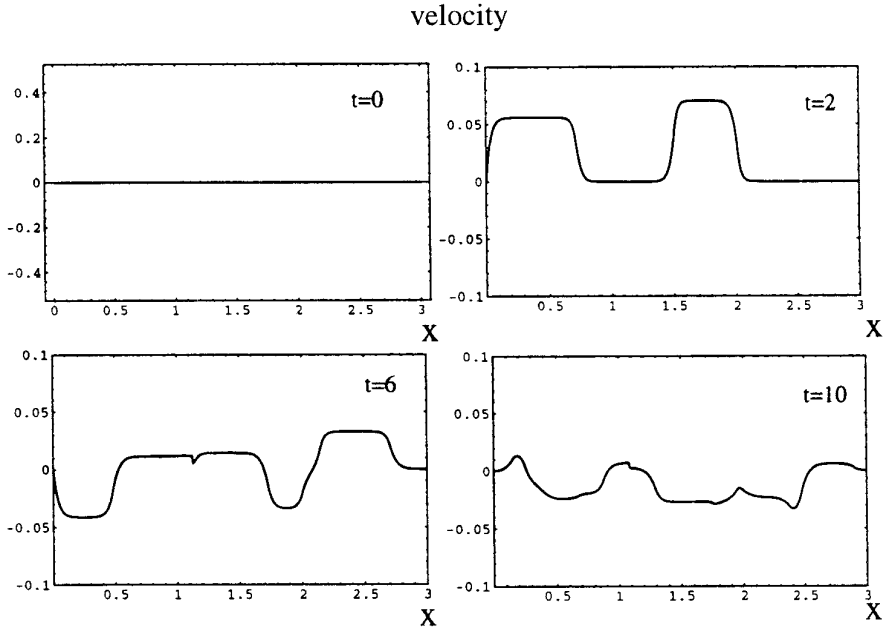

FIG. 26. The particle velocity velocity distribution in a finite bar at different time.

method is shown to be consistent, entropically admissible, and convergent. In our method, a phase boundary is tracked explicitly and a shock wave or contact discontinuity is captured. For trilinear materials, shock waves are degenerated to contact discontinuities, and thus they are smeared out slightly. For nonlinear two-phase materials (Test 7), a real shock is captured accurately. In this case, even a first-order method can give a relatively sharp shock front. Our preliminary tests show that the proposed methods are capable of approximating the initial-boundary value problems of the Abeyaratne–Knowles model.

In our numerical methods, a locally nonuniform and time-dependent mesh is used in the tracking/capturing method. The mesh technique is straightforward and easy to implement. On the other hand, our method requires the phase boundary to be a grid point. This requirement may limit its feasibility in multidimensional applications. We are currently working to improve our method so that the phase boundaries need not be explicitly tracked. A possible approach is to use the subcell resolution technique developed for shock capturing (see, e.g., [29, 46, 47]). In particular, the work of Mao [46, 47] can be used naturally in our context. In [46, 47], the *critical cell* that contains a discontinuity is tracked, but not the discontinuity itself. This "tracking" technique is much more robust than the conventional tracking methods, and it can be applied to two-dimensional cases in a dimension-by-dimension way [48]. With some modifications, this "tracking" technique can be applied to the computation of propagating phase boundaries when the kinetic relation is appropriately incorporated into the numerical scheme. More work is necessary for the application of this "tracking" technique to the phase boundary problems in complicated situations, such the nucleation of new phases. This investigation is in progress.

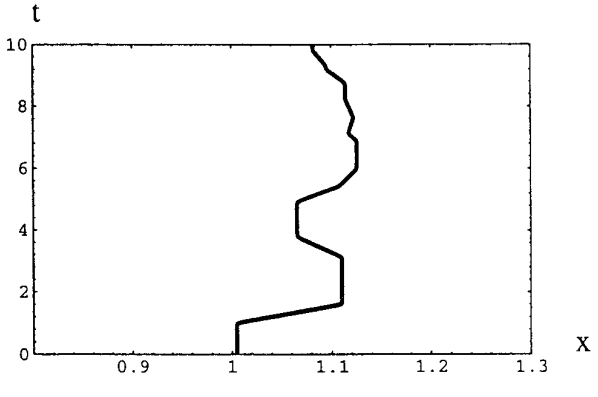

FIG. 27. Trajectory of the phase boundary in a finite bar.

We also propose an approximate Riemann solver to compute the propagating phase boundaries for general two-phase elastic materials. The Roe's type of approximate Riemann solver gives a reasonably good approximation to the exact Riemann solution. But it does not seem to converge under mesh refinement. We find it most effective to use the Roe-type of approximate Riemann solver along with the iterative exact Riemann solver based on the Newton iteration. We use the approximate Riemann solution as our initial guess for the iterative Riemann solver. This gives a fast convergent method to compute the exact Riemann solution.

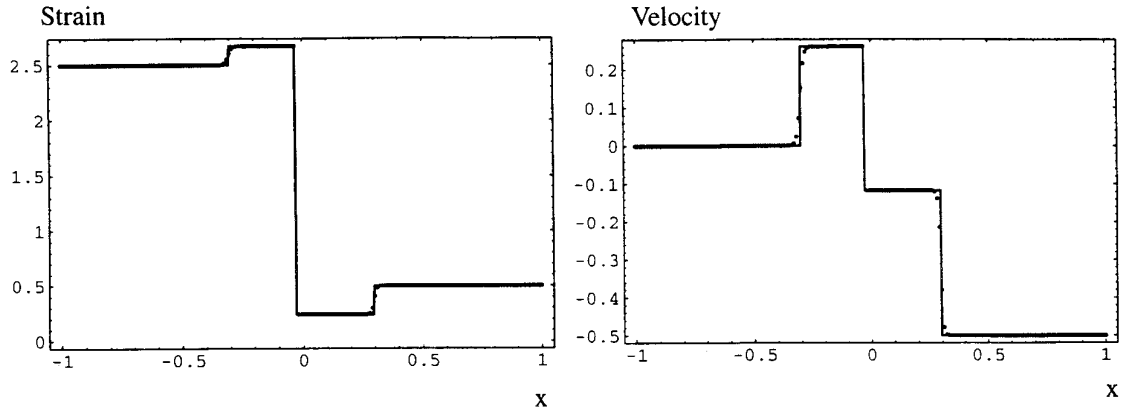

FIG. 28. Solutions to a Riemann problem with 3–1 initial data: (a) the strain distribution; (b) the particle velocity distribution.

Glimm's scheme produces relatively large errors for complicated initial-boundary value problems (Test 5), but it can deliver fairly good results for the propagation of a single phase boundary. Also, Glimm's scheme is easy to implement. It produces sharp phase boundaries, sharp contact discontinuities, and shock fronts. Another advantage of Glimm's scheme is that we can use a fixed mesh, instead of a moving mesh. One way to take advantage of Glimm's scheme is to combine Glimm's scheme with other high order methods, and to use Glimm's scheme at a phase boundary, but high order methods away from the phase boundaries. This work is in progress.

APPENDIX A: INITIAL VALUE PROBLEM FOR THE PROPAGATION OF A SINGLE PHASE BOUNDARY

Now we consider an initial value problem for the propagation of a single phase boundary for trilinear materials. The initial data are of the following form:

$$v(x,0), \gamma(x,0) = \begin{cases} v_L(x), \gamma_L(x), & x < 0, \\ v_R(x), \gamma_R(x), & 0 < x. \end{cases} \quad \text{(A1.1)}$$

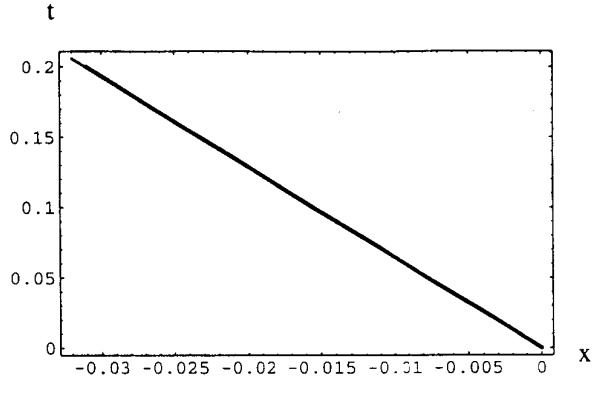

FIG. 29. Trajectory of the phase boundary.

Here $v_L(x)$, $v_R(x)$, $\gamma_L(x)$, and $\gamma_R(x)$ are continuous functions. We require that $\gamma_L(x) \in (-1, \gamma_m)$ and $\gamma_R(x) \in (\gamma_M, \infty)$; i.e., $\gamma_L(x)$ is in the low strain phase (phase 1) and $\gamma_R(x)$ is in the high strain phase (phase 3). For simplicity, we further require that the variations of $v_L(x)$, $v_R(x)$, $\gamma_L(x)$, and $\gamma_R(x)$ should be small and their values should be small enough in their ranges so that there is no new phase boundary nucleated at any time.

There is no self-similar solution to this initial value problem. However, we can solve the problem by the characteristics method. For trilinear materials, the characteristic lines of the partial differential equations under consideration are straight lines in both hyperbolic regions (high strain regions and low strain regions): $x \pm ct = \text{const}$.

Assume that the trajectory of the phase boundary initially $x = 0$ is $x = s(t)$ with $s(0) = 0$. It can be shown by jump conditions and entropy conditions at the phase boundary that $-ct < s(t) < ct$. We can determine $v^-(x, t)$, $\gamma^-(x, t)$ for $x + ct < 0$ and $v^+(x, t)$, $\gamma^+(x, t)$ for $x + ct > 0$ by Riemann invariants; however, we cannot determine $v(x, t)$ and $\gamma(x, t)$ in the fan area $-ct < x < ct$, because the characteristics lines cannot carry information through the phase boundary.

For $-ct < x < s(t)$,

$$v^-(x,t) - c\gamma^-(x,t) = v_L(x_0) - c\gamma_L(x_0), \quad \text{(A1.2)}$$

where $x - ct = x_0$.

For $s(t) < x < ct$,

$$v^+(x,t) + c\gamma^+(x,t) = v_R(x_0) + c\gamma_R(x_0), \quad \text{(A1.3)}$$

where $x + ct = x_0$.

To determine $v^{\pm}(s(t) \pm, t)$ and $\gamma^{\pm}(s(t) \pm, t)$, we have the following equations from Riemann invariants, jump conditions, and kinetic relations at the phase boundary $x = s(t)$:

$$v^-(s(t),t) - c\gamma^-(s(t),t) = v_L(x_0) - c\gamma_L(x_0);$$
$$x_0 = s(t) - ct, \tag{A1.4}$$
$$v^+(s(t),t) + c\gamma^+(s(t),t) = v_R(y_0) + c\gamma_R(y_0);$$
$$y_0 = s(t) + ct, \tag{A1.5}$$
$$v^+(s(t),t) - v^-(s(t),t) + \dot{s}(t)(\gamma^+(s(t)\cdot t) - \gamma^-(s(t),t)) = 0, \tag{A1.6}$$
$$\mu(\gamma^+(s(t),t) - \gamma_T) - \mu\gamma^-(s(t),t) + \rho\dot{s}(t)(v^+(s(t)\cdot t) - v^-(s(t),t)) = 0, \tag{A1.7}$$
$$\frac{\mu\gamma_T}{2}(\gamma_m + \gamma_M - \gamma^+(s(t)\cdot t) - \gamma^-(s(t),t)) = \omega\dot{s}(t), \tag{A1.8}$$

with $s(0) = 0$.

From Eqs. (A1.4)–(A1.8), we can obtain a single equation for $s(t)$,

$$\frac{c\dot{s}(t)\gamma_T}{c^2 - \dot{s}^2(t)} + \frac{2\omega\dot{s}(t)}{\mu\gamma_T} + \frac{v_R(s(t)+ct) + c\gamma_R(s(t)+ct) - v_L(s(t)-ct) + c\gamma_L(s(t)-ct)}{c} - \gamma_m - \gamma_M = 0, \tag{A1.9}$$

with $s(0) = 0$.

If $s(t)$ is determined from (A1.9), we can solve for $v^{\pm}(s(t)\pm, t)$ and $\gamma^{\pm}(s(t)\pm, t)$ from Eqs. (A1.4)–(A1.7). Once these quantities are determined, all the variables in the fan areas, $-ct < x < s(t)$ and $s(t) < x < ct$, can be determined by Riemann invariants in these areas. However, this highly nonlinear ordinary differential equation is impossible to solve analytically. We solve it here by iteration and approximation:

1. $t = 0$, (A1.9) reduces to

$$\frac{c\dot{s}(0)\gamma_T}{c^2 - \dot{s}^2(0)} + \frac{2\omega}{\mu\gamma_T}\dot{s}(0) + (v_R(0) + c\gamma_R(0) - v_L(0) + c\gamma_L(0))/c - \gamma_m - \gamma_M = 0, \tag{A1.10}$$

a algebraic equation for $\dot{s}(0)$; $\dot{s}(0)$ can be determined.

2. $t_n = n\ \Delta t$, $s(t_n) = s(t_{n-1}) + \dot{s}(t_{n-1})\ \Delta t$. Then we substitute $s(t_n)$ into (A1.9), and we obtain a new algebraic equation for $\dot{s}_{t_n}$. We can determine $\dot{s}_{t_n}$. Subsequently, we can solve for $v^{\pm}(s(t_n), t_n)$ and $\gamma^{\pm}(s(t_n), t_n)$ from Eqs. (A1.4)–A1.7).

It is cumbersome to determine all the variables in the fan areas $-ct < x \leq s(t)$ and $s(t) < x < ct$. Test 2 in Section 6.2 shows that our numerical method delivers solutions almost identical to those obtained by the characteristics method presented here.

ACKNOWLEDGMENTS

The authors are grateful to Professor James K. Knowles for his interest in this work and his encouragement. We appreciate the referees' comments on an earlier version of the manuscript. We are especially grateful to one referee who brought our attention to Mao's work and suggested additional numerical tests. T.Y.H. was partially supported by AFOSR Grant F49620-94-1-0215. P.G.L. was partially supported by NSF Grants DMS-92-09326 and DMS-94-09400, and AFOSR Grant F49620-94-1-0215. X.Z. was supported by ONR Grant N0014-93-1-0240.

REFERENCES

1. R. Abeyaratne, *J. Elasticity* **10,** 255 (1980).
2. R. Abeyaratne and J. K. Knowles, *Int. J. Solids Struct.* **24,** 1021 (1988).
3. R. Abeyaratne and J. K. Knowles, *J. Mech. Phys. Solids* **38,** 345 (1990).
4. R. Abeyaratne and J. K. Knowles, *Arch. Rat. Mech. Anal.* **114,** 119 (1990).
5. R. Abeyaratne and J. K. Knowles, *SIAM J. Appl. Math.* **51,** 1205 (1991).
6. M. Affouf and R. Caflisch, *SIAM J. Appl. Math.* **51,** 605 (1991).
7. J. Ball and R. D. James, *Arch. Rat. Mech. Anal.* **100,** 13 (1986).
8. M. J. Berger and P. Colella, *J. Comput. Phys.* **82,** 64 (1989).
9. M. J. Berger and J. Oliger, *J. Comput. Phys.* **53,** 484 (1984).
10. K. Bhattacharya, *Acta Metal.* **39,** 2431 (1991).
11. A. Bourlioux, A. J. Majda, and V. Roytburds, *SIAM J. Appl. Math.* **51,** 303 (1991).
12. I.-L. Chern and P. Colella, UCRL-97200, Lawrence Livermore National Laboratories 1987 (unpublished).
13. J. W. Christian, *Theory of Transformation in Metals and Alloys, Part I* (Pergamon, Oxford, 1975).
14. B. Cockburn and H. Gau, Preprint, IMA, Minneapolis, 1994; *SIAM J. Sci. Stat. Comput.,* submitted.
15. P. Colella, Glimm's method for gas dynamics, *SIAM J. Sci. Stat. Comput.* **3,** 76 (1982).
16. P. Colella and P. R. Woodward, *J. Comput. Phys.* **54,** 174 (1984).
17. C. Collins and M. Luskin, The computation of the austenite–marstenite phase transitions, in Lect. Notes in Physics, Vol. 344, edited by M. Rascle, D. Serre, and M. Slemrod (Springer-Verlag, New York/Berlin, 1989), p. 34.
18. C. M. Dafermos, *Systems of Nonlinear Partial Differential Equations* edited by J. M. Ball, NATO-ASI Series C, Vol. 111 (Reidel, Dordrecht, 1983), p. 25.
19. J. L. Ericksen, *J. Elasticity* **5,** 191 (1975).
20. H. T. Fan and M. Slemrod, in *Shock Induces Transitions and Phase Structures in General Media,* edited by R. Fosdick, E. Dunn, and H. Slemrod, IMA Vol. Math. Appl. 52 (Springer-Verlag, New York/Berlin, 1993).
21. M. E. Fine, *Introduction to Phase Transformations in Condensed Systems* (Macmillan Co., New York, 1975).
22. J. Glimm, Solutions in the large for nonlinear hyperbolic systems of equations, *Commun. Pure Appl. Math.* **18,** 697 (1965).
23. J. Glimm and P. D. Lax, *Mem. Am. Math. Soc.* **101,** (1970).
24. J. Glimm, E. Isaacson, D. Marchesin, and O. A. McBryan, *Adv. Appl. Math.* **2,** 91 (1981).

25. J. Glimm, C. Klingenberg, O. McBryan, B. Plohr, and D. Sharp, Front tracking and two-dimensional Riemann problems, *Adv. Appl. Math.* **6,** 259 (1985).
26. S. K. Godunov, *Mat. Sb.* **47,** 271 (1959).
27. A. Harten and J. M. Hyman, *J. Comput. Phys.* **50,** 235 (1983).
28. A. Harten, *J. Comput. Phys.* **49,** 357 (1983).
29. A. Harten, *J. Comput. Phys.* **83,** 148 (1987).
30. A. Harten and S. J. Osher, *SIAM J. Numer. Anal.* **24,** 279 (1987).
31. T. Y. Hou and P. G. LeFloch, *Math. Comput.* **62,** 497 (1994).
32. J. M. Hyman, *Physica D* **12,** 396 (1984).
33. E. Isaacson, D. Marchesin, and B. Plohr, *SIAM J. Math. Anal.* **21,** 837 (1990).
34. R. D. James, The propagation of phase boundaries in elastic bars, *Arch. Rat. Mech. Anal.* **73,** 125 (1980).
35. S. Jin, *SIAM J. Appl. Math.,* to appear.
36. B. L. Keyfitz, *Lect. in Appl. Math.,* Vol. 23 (Am. Math. Soc., Providence, RI, 1986), p. 379.
37. P. Kloucek and M. Luskin, *Cont. Mech. Therm.* **6,** 209 (1994).
38. J. K. Knowles, *J. Elasticity* **9,** 131 (1979).
39. P. D. Lax, ''Hyperbolic Systems of Conservation Laws and the Mathematical Theory of Shock Waves,'' Regional Conf. Series in Appl. Math., Vol. 11 (SIAM, Philadelphia, 1973).
40. B. van Leer, *J. Comput. Phys.* **32,** 101 (1979).
41. P. G. LeFloch, *Arch. Rat. Mech. Anal.* **123,** 153 (1993).
42. R. J. LeVeque and K. M. Shyue, Research Report 91-02, ETH, Zurich, 1991 (unpublished).
43. Y. Lin, *Quart. Appl. Math.,* to appear.
44. T. P. Liu and K. Zumbrun, preprint, 1994.
45. E. N. Mamiya and J. C. Simo, *J. Elasticity* **35,** 175 (1994).
46. D. K. Mao, *J. Comput. Phys.* **92,** 422 (1991).
47. D. K. Mao, *J. Comput. Phys.* **103,** 359 (1992).
48. D. K. Mao, *J. Comput. Phys.* **104,** 377 (1993).
49. G. Moretti, *Comput. & Fluids* **15,** 59 (1987).
50. R. A. Nicolaides and N. J. Walkington, in *Recent Advances in Adaptive and Sensory Materials and Their Applications* edited by C. A. Rogers and R. C. Rogers 1992, p. 131.
51. E. S. Oran and J. P. Boris, *Numerical Simulations of Reactive Flow* (Technomic, Lancaster, PA, (Elsevier, New York, 1987).
52. S. J. Osher, *SIAM J. Num. Anal.* **22,** 947 (1985).
53. P. L. Roe, *J. Comput. Phys.* **43,** 357 (1981).
54. P. Rosakis, *Arch. Rat. Mech. Anal.* **109,** 1 (1990).
55. P. Rybka, *Proc. R. Soc. Edinburgh A* **121,** 101 (1992).
56. M. Shearer, The Riemann problem for a class of conservation laws of mixed type, *J. Differential Equations* **46,** 426 (1982).
57. C.-W. Shu and S. Osher, CAM Report 88-12, UCLA, April 1988 (unpublished).
58. K-M. Shyue, Ph.D. thesis, University of Washington, Seattle, 1993 (unpublished).
59. S. A. Silling, *J. Elasticity* **19,** 213 (1988).
60. S. A. Silling, *J. Elasticity* **28,** 143 (1992).
61. M. Slemrod, in *Physical Mathematics and Nonlinear PDE's,* edited by S. M. Rankin and J. M. Lightbourne (Dekker, New York, 1985).
62. P. J. Swart and P. Holmes, *Arch. Rat. Mech. Anal.* **121,** 37 (1992).
63. L. Truskinovsky, in *Shock Induces Transitions and Phase Structures in General Media,* edited by R. Fosdick, E. Dunn, and H. Slemrod, IMA Math. Appl., Vol. 52 (Springer-Verlag, New York/Berlin, 1993).
64. J. H. Weiner, in *Proceedings Sixth U.S. National Congress of Applied Mechanics,* edited by G. Carrier (ASME, New York, 1970), p. 62.
65. X.-G. Zhong, Ph.D. thesis, California Institute of Technology, Pasadena, May 1995.